

# WELL-CENTERED TRIANGULATION¶

EVAN VANDERZEE\*, ANIL N. HIRANI†, DAMRONG GUOY‡, AND EDGAR A. RAMOS§

**Abstract.** Meshes composed of well-centered simplices have nice orthogonal dual meshes (the dual Voronoi diagram). This is useful for certain numerical algorithms that prefer such primal-dual mesh pairs. We prove that well-centered meshes also have optimality properties and relationships to Delaunay and minmax angle triangulations. We present an iterative algorithm that seeks to transform a given triangulation in two or three dimensions into a well-centered one by minimizing a cost function and moving the interior vertices while keeping the mesh connectivity and boundary vertices fixed. The cost function is a direct result of a new characterization of well-centeredness in arbitrary dimensions that we present. Ours is the first optimization-based heuristic for well-centeredness, and the first one that applies in both two and three dimensions. We show the results of applying our algorithm to small and large two-dimensional meshes, some with a complex boundary, and obtain a well-centered tetrahedralization of the cube. We also show numerical evidence that our algorithm preserves gradation and that it improves the maximum and minimum angles of acute triangulations created by the best known previous method.

**Key words.** well-centered, meshing, mesh optimization, acute, triangulation, discrete exterior calculus

**AMS subject classifications.** 65N50, 65M50, 65D18, 51M04

**1. Introduction.** A *completely well-centered* mesh is a simplicial mesh in which each simplex contains its circumcenter in its interior. A 3-dimensional example is a tetrahedral mesh in which the circumcenter of each tetrahedron lies inside it and the circumcenter of each triangle face lies inside it. Weaker notions of well-centeredness require that simplices of specific dimensions contain their circumcenters. In two dimensions, a completely well-centered triangulation is the same thing as an acute triangulation.

Typical meshing algorithms do not guarantee well-centeredness. For example, a Delaunay triangulation is not necessarily well-centered. In this paper we discuss well-centered triangulations, with particular application to triangle and tetrahedral meshes. We present an iterative energy minimization approach in which a given mesh, after possible preprocessing, may be made well-centered by moving the internal vertices while keeping the boundary vertices and connectivity fixed.

A well-centered (primal) mesh has a corresponding dual mesh assembled from a circumcentric subdivision [23]. For an  $n$ -dimensional primal mesh, a  $k$ -simplex in the primal corresponds to an  $(n - k)$ -cell in the dual. For example, in a well-centered

---

¶Preliminary results for the 2-dimensional problem of well-centered planar triangulations appeared previously in the Proceedings of the 16th International Meshing Roundtable, Seattle, WA, October 14-17, 2007 [40].

\*Department of Mathematics, 1409 W. Green Street, University of Illinois at Urbana-Champaign, Urbana, IL 61801 (vanderze@illinois.edu). Research supported by CSE Fellowship from the Computational Science and Engineering Program and Applied Mathematics Program, University of Illinois and by NSF CAREER Award, Grant No. DMS-0645604.

†Author for Correspondence, Department of Computer Science, 201 N. Goodwin Avenue, University of Illinois at Urbana-Champaign, Urbana, IL 61801 (hirani@illinois.edu). Research supported by NSF CAREER Award, Grant No. DMS-0645604.

‡Computational Science and Engineering Program, Center for Simulation of Advanced Rockets, University of Illinois at Urbana-Champaign now at Synopsys Inc., Mountain View, California (Damrong.Guoy@synopsys.com)

§Escuela de Matemáticas, Universidad Nacional de Colombia, Medellín, Colombia (earamosn@unalmed.edu.co)

planar triangle mesh, the dual of a primal interior vertex is a convex polygon with boundary edges that are orthogonal and dual to primal edges. This orthogonality makes it possible to discretize the Hodge star operator of exterior calculus [1] as a diagonal matrix, simplifying certain computational methods for solving partial differential equations and for topological calculations. Some numerical methods that mention well-centered meshes in this context are the covolume method [29] and Discrete Exterior Calculus [10, 23].

Well-centered meshes are not strictly required for these or other related methods; however, some computations would be easier if such meshes were available. For example, a stable mixed method for Darcy flow has recently been derived using Discrete Exterior Calculus [24] and applied to well-centered meshes generated by our code and to Delaunay meshes. That numerical method passes patch tests in 2 and 3 dimensions for both homogeneous and heterogeneous problems. Figure 1.1 (reproduced from [24] by permission of the authors) shows the velocities from a solution to the Darcy flow problem in a layered medium. The solution was computed with that numerical method and a well-centered mesh.

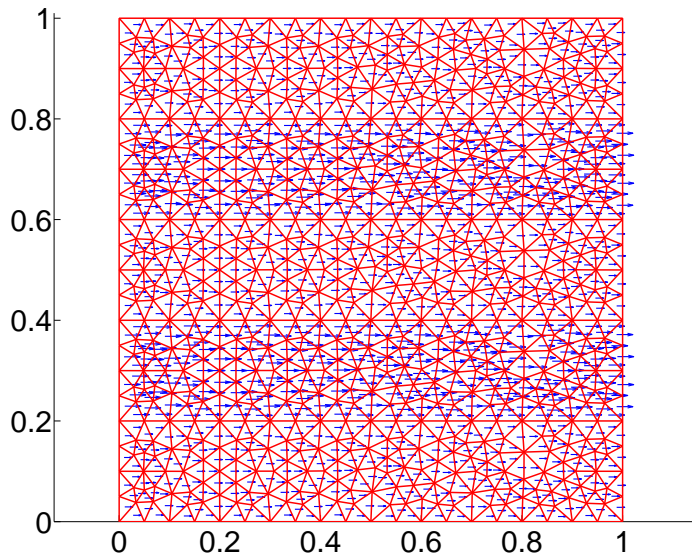


FIG. 1.1. Darcy flow in a medium with 5 layers, computed on a well-centered mesh. The odd layers have a permeability of 5 and even layers have permeability of 10. The velocities in the odd and even layers should be different and should have no vertical component, as shown. The mesh was created using our code. Figure taken from [24], used by permission from authors.

In the case of covolume methods applied to Maxwell’s equations, a justification for well-centered triangulation is given in [32, 33, 34, 35].

Another example from scientific computing is space-time meshing. When tent-pitching methods for space-time meshing were first introduced, the initial spatial mesh was required to be acute, which for two-dimensional meshes is the same thing as being well-centered [38]. More recently this requirement has been avoided, although at the expense of some optimality in the construction [20].

In two dimensions, well-centered meshes achieve optimality in *two* objectives that are important in some applications. If a planar point set has a well-centered triangulation, that triangulation both *minimizes* the *maximum* angle and *maximizes* the

*minimum* angle. We don't know any generalizations of this double optimality to higher dimensions, but it is known that in any dimension if the convex hull of a point set has a well-centered triangulation, then that triangulation is unique and it is the Delaunay triangulation [30].

**2. Our Results.** We *characterize* well-centered triangulations in arbitrary dimensions, *prove optimality* results for two-dimensional well-centered triangulations, and give many experimental results.

The new characterization of well-centeredness that we give here is a useful theoretical tool that allows us to relate well-centeredness and Delaunay triangulation in arbitrary dimensions. In addition, it is also a practical tool since it presents, for the first time, a path to the creation of higher-dimensional well-centered triangulations. Even the formulation of an optimization approach for higher-dimensional well-centeredness would be difficult without such a characterization. Indeed, ours is the first algorithm to even consider using an optimization approach to seek well-centeredness. This approach allows us both to improve existing triangulations in  $\mathbb{R}^2$  and to create well-centered triangulations in  $\mathbb{R}^3$ . We also prove optimality results about our cost function and optimality results that relate well-centeredness to well-known triangulation schemes. The specific results are enumerated below.

(a) We introduce a new characterization of well-centeredness in arbitrary dimensions (Thm. 4.1). (b) As a simple corollary (Cor. 4.2) we show that for any dimension  $n$ , an  $n$ -well-centered triangulation of a convex subset of  $\mathbb{R}^n$  is Delaunay, which is a new proof of a result in [30]. (c) Using the characterization of Thm. 4.1 we define a family of cost functions  $E_p$  (equation 5.2) suitable for creating well-centered triangulations in arbitrary dimensions. (d) With these we design an algorithm that optimizes meshes with the goal of producing well-centered meshes. The algorithm generalizes our previous angle-based optimization in two dimensions, described in [40]. *Ours is the first known strategy for well-centeredness that generalizes to higher dimensions.* (e) Using the algorithm we produce a well-centered triangulation of a cube (Fig. 7.12). (f) We show several two dimensional examples, including one with more than 60000 triangles (middle of Fig. 7.11). (g) In two dimensions, every algorithm proven to generate acute triangulations may produce angles arbitrarily close to  $\pi/2$ . Moreover, in all cases we have tried, *our optimization algorithm can improve the quality of planar acute-angled triangulations produced by other heuristics for creating acute triangulations.* A challenging example is shown in Fig. 7.9. (h) We also demonstrate numerically that *graded triangulations maintain their gradation while being processed by our algorithm* (Fig. 7.3, 7.8, 7.9). This is useful since producing provably acute graded triangulations is an open problem. (i) For planar triangulations, we show that the *minmax triangulation [17] is the optimal triangulation with respect to our energy  $E_\infty$*  (Cor. 6.3). (j) We give a different proof for the acute angle case of a result from [4]; we show that if a planar point set admits a 2-well-centered triangulation, then that triangulation is the unique Delaunay triangulation and the unique minmax triangulation of the point set (Thm. 6.4).

Our *experimental* results in three dimensions are rudimentary, although even these were not available before our work. The difficulty in three dimensions lies further upstream, in a step that precedes the application of our optimization algorithm. In the planar case, an interior vertex with four neighbors must be incident to an obtuse triangle, but some simple connectivity preprocessing can fix this problem [40]. Similarly, a tetrahedral mesh may have topological obstructions to well-centeredness. The topological obstructions in this case, however, are not yet fully understood. Some

progress has been made in our other work [41] by studying the link of (topological sphere around) a vertex, but much remains to be done. The techniques used to study such topological obstructions are interesting, but they are transversal to this paper.

**3. Previous Results.** We are concerned with triangulations for which the domain is specified by a polygonal or polyhedral boundary. Our main objective is obtaining well-centered triangle and tetrahedral meshes. Relevant work can be divided into constructive and iterative approaches.

Constructive approaches start with specified input constraints and generate additional points, called Steiner points, and/or a corresponding triangulation. Normally a point is committed to a position and never moved afterwards. An algorithm for nonobtuse planar triangulations based on circle packings is described in [3]. More recent works describe improved constructions for nonobtuse triangulations while also describing how to derive an acute triangulation from a nonobtuse one [26, 44]. There are two major difficulties with such methods. The first is that these algorithms aim to achieve a triangulation of size linear in the input size. As a result, the *largest and smallest angles can be arbitrarily close to  $\pi/2$  and 0 respectively*. The second major difficulty with these algorithms is that they *do not offer a clear path towards a higher-dimensional generalization*. Moreover, we are not aware of any existing implementations of these algorithms, which seem to be primarily of theoretical interest. As recently as 2007, Erten and Üngör [21] proposed a variant of the Delaunay refinement algorithm for generating acute triangulations of planar domains. This heuristic, which relocates Steiner points after they are added, has been implemented and appears to work quite well. Experiments suggest, however, that the maximum angle in the output is often near  $\pi/2$ , and our method is able to improve their meshes. See, for example, the mesh of Lake Superior in Section 7.

There is also a constructive algorithm that achieves a well-centered quality triangulation of a point set [5] (with no polygonal boundary specified), and an algorithm for constructing nonobtuse quality triangulations [27]. Also relevant is an algorithm that, given a constraint set of both points and segments in the plane, finds a triangulation that minimizes the maximum angle [17], without adding points. If an acute triangulation exists for the input constraints, the algorithm will find one. The most promising of the constructive algorithms is probably [21] mentioned above. But for this algorithm, as well as for the others mentioned in this paragraph, we are not aware of higher-dimensional generalizations.

Yet another approach is the mesh stitching approach in [32, 34, 35]. In this scheme, the region near the boundary and the interior far from boundary are meshed separately and these two regions are stitched with a special technique. However, in three dimensions, the method is unable to generate a well-centered triangulation in their examples [32].

On the other hand, there are iterative or optimization approaches which allow an initial triangulation (possibly the canonical Delaunay) and then move the points while possibly changing the connectivity. These algorithms often apply in three dimensions as well as two. Moreover, there are many well-known existing meshing algorithms, some of which generate quality triangulations [15, 31] and have reliable implementations. An iterative approach can start from an existing high-quality mesh and seek to make it well-centered while retaining its high quality.

In the class of iterative approaches there are optimization methods like centroidal Voronoi tessellations [12, 13, 14], variational tetrahedral meshing [2]. Each of these methods has a global cost function that it attempts to minimize through an iterative

procedure that alternates between updating the location of the mesh vertices and the triangulation of those vertices. Our algorithm has some similarities to these methods, but uses a cost function explicitly designed to seek well-centered simplices, in contrast to the cost functions optimized in [12] and [2].

There are also many iterative optimization methods that, like our method, relocate vertices without changing the initial mesh connectivity. Traditional Laplacian smoothing[43] is one such method. Such methods improve meshes according to some criteria, but do not typically produce well-centered meshes. (See, for example, our comparisons with Laplacian smoothing in Sections 7.5 and 7.7.)

In addition to optimization approaches that work directly with a mesh, there are several algorithms that generate circle packings or circle patterns by optimizing the radii of the circles. In particular, the algorithms for creating circle patterns that were proposed in [9] and [6] can be adapted to create triangulations. These algorithms produce circle patterns that have specified combinatorics, but they do not permit a complete specification of the domain boundary, so they are not appropriate to our purpose.

The problem of generating a well-centered tetrahedralization in  $\mathbb{R}^3$  is considerably harder than the two-dimensional analogue. A complete characterization of the topological obstructions to well-centeredness in three dimensions is still an open problem, although a start has been made in our work elsewhere [41]. Similarly, the problem of generating a three-dimensional acute triangulation—a tetrahedralization in which all the dihedral angles are acute—is more difficult than generating a two-dimensional acute triangulation. For tetrahedra, it is no longer true that well-centeredness and acuteness are equivalent [39, Section 2]. In addition, acute tetrahedralizations are known for only restricted domains. For example, until recently it was not known whether the cube has an acute triangulation. The construction that showed the cube does have an acute triangulation made use of the well-centered optimization discussed in this paper [42].

**4. Characterization of Well-Centeredness.** We begin with a new characterization of well-centeredness in arbitrary dimension. This characterization allows us to create an algorithm, described in Section 5, that uses optimization to seek well-centeredness. It also serves, later in the current section, as a theoretical tool in relating arbitrary-dimensional well-centeredness to Delaunay triangulations.

Consider an  $n$ -dimensional simplex  $\sigma^n$  embedded in Euclidean space  $\mathbb{R}^m$ ,  $m \geq n$ . The affine hull of  $\sigma^n$ ,  $\text{aff}(\sigma^n)$ , is the smallest affine subspace of  $\mathbb{R}^m$  that contains  $\sigma^n$ . In this case,  $\text{aff}(\sigma^n)$  is a copy of  $\mathbb{R}^n$  embedded in  $\mathbb{R}^m$ . The circumcenter of  $\sigma^n$ , which we denote  $c(\sigma^n)$ , is the unique point in  $\text{aff}(\sigma^n)$  that is equidistant from every vertex of  $\sigma^n$ .

For an  $n$ -simplex  $\sigma^n$  with  $n \geq 3$ , it is possible for  $\sigma^n$  to contain its circumcenter  $c(\sigma^n)$  while some proper face  $\sigma^p \prec \sigma^n$  does not contain its circumcenter  $c(\sigma^p)$ . It is also possible that for all  $1 \leq p < n$  and all  $\sigma^p \prec \sigma^n$ ,  $c(\sigma^p)$  lies in the interior of  $\sigma^p$ , but  $\sigma^n$  does not contain its circumcenter. (See [39] for examples with  $n = 3$ .) Thus we say that an  $n$ -simplex  $\sigma^n$  is a  $(p_1, \dots, p_k)$ -well-centered simplex if for  $p_i$ ,  $i = 1, \dots, k$ , all faces of  $\sigma^n$  of dimension  $p_i \leq n$  properly contain their circumcenters. The parentheses are suppressed when referring to only one dimension. A simplex  $\sigma^n$  is *completely well-centered* if it is  $(1, 2, \dots, n-1, n)$ -well-centered.

In this section we give an alternate characterization for an  $n$ -simplex  $\sigma^n$  that is  $n$ -well-centered. The characterization, which shows how the  $n$ -well-centered  $n$ -simplex generalizes the acute triangle to higher dimensions, uses the concept of an equatorial

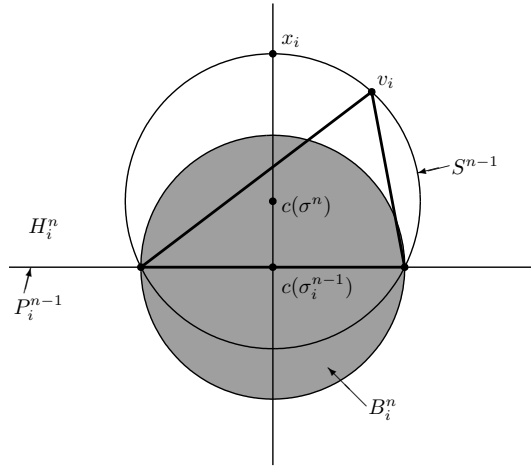


FIG. 4.1. An illustration of the proof of Theorem 4.1 in two dimensions. In an  $n$ -well-centered simplex  $\sigma^n$ , vertex  $v_i$  and circumcenter  $c(\sigma^n)$  lie in the same open half-space  $H_i^n$ , the region where circumsphere  $S^{n-1}$  lies outside equatorial ball  $B_i^n$ .

ball, which we now define.

Let  $\sigma^n$  be a simplex embedded in a hyperplane  $P^m$  with  $m > n$ . The *equatorial ball* of  $\sigma^n$  in  $P^m$  is the closed ball  $\{x \in P^m : |x - c(\sigma^n)| \leq R(\sigma^n)\}$ , where  $c(\sigma^n)$  is the circumcenter of  $\sigma^n$ ,  $R(\sigma^n)$  its circumradius, and  $|\cdot|$  the standard Euclidean norm. In this paper we use the notation  $B(\sigma^n)$  for the equatorial ball of  $\sigma^n$ . The notation is used in the context of  $\sigma^n \prec \sigma^{n+1}$ , and the hyperplane  $P^m$  is understood to be  $\text{aff}(\sigma^{n+1})$ . The equatorial ball is an extension of the circumball into higher dimensions; it is assumed throughout this paper that the *circumball* and *circumsphere* of a simplex  $\sigma^n$  are embedded in  $\text{aff}(\sigma^n)$ . Note that here and throughout the paper we have implicitly assumed that an  $n$ -simplex is fully  $n$ -dimensional, though when a simplicial mesh is represented on a computer it may be the case that some of the simplices are degenerate.

**THEOREM 4.1.** *The  $n$ -simplex  $\sigma^n = v_0v_1 \dots v_n$  is  $n$ -well-centered if and only if for each  $i = 0, 1, \dots, n$ , vertex  $v_i$  lies strictly outside  $B_i^n := B(v_0v_1 \dots v_{i-1}v_{i+1} \dots v_n)$ .*

*Proof.* Figure 4.1 illustrates this proof in dimension  $n = 2$ . It may help the reader understand the notation used in the proof and give some intuition for what the proof looks like in higher dimensions.

First we suppose that  $\sigma^n$  is  $n$ -well-centered. Let  $S^{n-1} = S^{n-1}(\sigma^n)$  be the circumsphere of  $\sigma^n$ . Now  $\text{aff}(\sigma^n)$  is a copy of  $\mathbb{R}^n$ , and within that copy of  $\mathbb{R}^n$ ,  $\sigma^n$  is an intersection of half-spaces. Considering some particular vertex  $v_i$  of  $\sigma^n$ , we know that one of the bounding hyperplanes of  $\sigma^n$  is the hyperplane  $P_i^{n-1}$  that contains the simplex  $\sigma_i^{n-1} = v_0v_1 \dots v_{i-1}v_{i+1} \dots v_n$ .

Hyperplane  $P_i^{n-1}$  partitions our copy of  $\mathbb{R}^n$  into two half-spaces — an open half-space  $H_i^n$  that contains the interior of  $\sigma^n$  and vertex  $v_i$ , and a closed half-space that contains  $\sigma_i^{n-1}$  (on its boundary).

Because  $\sigma^n$  is well-centered,  $c(\sigma^n)$  lies in its interior. Thus  $c(\sigma^n)$  lies in  $H_i^n$ , the open half-space that contains  $v_i$ . Consider, then, the line through  $c(\sigma^n)$  and  $c(\sigma_i^{n-1})$ . Within  $H_i^n$ , this line intersects  $S^{n-1}$  at a point  $x_i$  with  $|x_i - c(\sigma^n)| = R(\sigma^n)$ . Moreover,  $|x_i - c(\sigma_i^{n-1})| > R(\sigma^n) > R(\sigma_i^{n-1})$ . We see that  $x_i$  lies outside  $B_i^n$  and conclude that

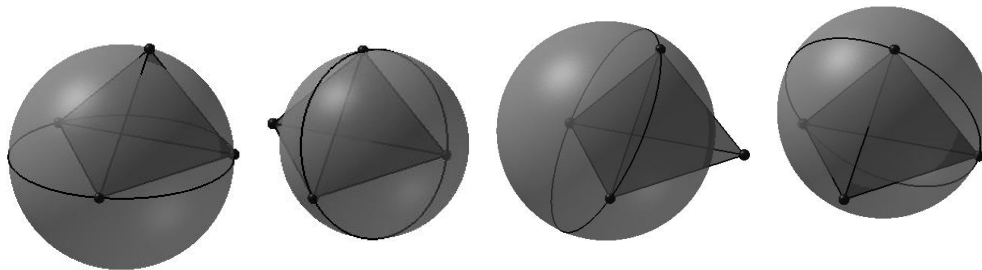


FIG. 4.2. One characterization of  $n$ -well-centeredness of an  $n$ -simplex  $\sigma^n$  is that for each vertex  $v_i$  of  $\sigma^n$ ,  $v_i$  lies outside of the equatorial ball  $B_i^n$  of the facet  $\sigma_i^n$  opposite  $v_i$ .

$S^{n-1} \cap H_i^n$  lies outside  $B_i^n$ . In particular, since  $v_i \in S^{n-1} \cap H_i^n$ , we know that  $v_i$  lies outside  $B_i^n$ . Since  $v_i$  was chosen arbitrarily, we conclude that  $v_i$  lies outside  $B_i^n$  for each  $i = 0, 1, \dots, n$ , and necessity is proved.

For sufficiency we consider an  $n$ -simplex  $\sigma^n$  such that  $v_i$  lies outside  $B_i^n$  for each  $i = 0, 1, \dots, n$ . We will show that the circumcenter  $c(\sigma^n)$  lies in the interior of  $\sigma^n$  by demonstrating that for each vertex  $v_i$ ,  $c(\sigma^n)$  lies in  $H_i^n$ . We know that  $P_i^{n-1}$  cuts  $S^{n-1}$  into a part inside  $B_i^n$  and a part outside  $B_i^n$ , and we have just established that whichever of the (open) half-spaces contains  $c(\sigma^n)$  is the half-space where  $S^{n-1}$  lies outside  $B_i^n$ . Since we are given that  $v_i \in S^{n-1}$  lies outside  $B_i^n$ , we know that  $v_i$  and  $c(\sigma^n)$  must lie in the same open half-space  $H_i^n$ . This holds for every  $v_i$ , so  $c(\sigma^n)$  is in the interior of  $\sigma^n$ , and  $\sigma^n$  is, by definition,  $n$ -well-centered.  $\square$

Figure 4.2 shows how Thm. 4.1 can be applied to a tetrahedron. In Fig. 4.2 we see that for each vertex  $v_i$  of the tetrahedron,  $v_i$  lies outside of equatorial ball  $B_i^n$ . By Thm. 4.1 we can conclude that the tetrahedron is 3-well-centered, even though we have not precisely located its circumcenter. This clearly generalizes the acute triangle; the angle at vertex  $v_i$  of a triangle is acute if and only if  $v_i$  lies outside  $B_i^n$ , and a triangle is 2-well-centered if and only if each of its angles is acute.

When we say that a mesh is a  $(p_1, \dots, p_k)$ -well-centered mesh, we mean that every element of the mesh is a  $(p_1, \dots, p_k)$ -well-centered simplex. In the proof of Thm. 4.1 we showed that for each face  $\sigma_i^{n-1}$  of an  $n$ -well-centered  $n$ -simplex  $\sigma^n$ , the hyperplane  $\text{aff}(\sigma_i^{n-1})$  cuts the circumball of  $\sigma^n$  into two pieces, one piece contained in  $B_i^n$  and the other piece lying on the same side of  $\text{aff}(\sigma_i^{n-1})$  as the interior of  $\sigma^n$ . It follows that the circumball of  $\sigma^n$  is contained in  $(\bigcup_i B_i^n) \cup \sigma^n$ . (It can be shown, in fact, that  $\sigma^n \subset \bigcup_i B_i^n$ , but we do not need that result here.) Moreover, if we consider some other  $n$ -well-centered  $n$ -simplex  $\tau^n$  such that  $\sigma_i^{n-1} = \tau^n \cap \sigma^n$ , and if vertex  $u$  is the vertex of  $\tau^n$  opposite  $\sigma_i^{n-1}$ , then Thm. 4.1 implies that  $u$  is outside  $B_i^n$ . Thus  $u$  also lies outside the circumball of  $\sigma^n$ . If the underlying space of the mesh is a convex subset of  $\mathbb{R}^n$ , we can conclude that the mesh is locally Delaunay. Since in any dimension a locally Delaunay mesh is globally Delaunay [16], we obtain a new proof of the following result, which was originally proved by Rajan [30].

**COROLLARY 4.2.** *If a simplicial mesh of a convex subset of  $\mathbb{R}^n$  is  $n$ -well-centered, then the mesh is a Delaunay triangulation of its vertices.*

The converse, of course, is not true. Section 6 gives more details for the planar

case.

**5. Iterative Energy Minimization.** Given a simplicial mesh, we seek to make the mesh well-centered by minimizing a cost function defined over the mesh. We'll refer to the cost function as *energy*. Our method is somewhat similar to the methods of [2] and [12] in that it uses an iterative procedure to minimize an energy defined on the mesh, but for reasons discussed in Section 6, it differs in that the mesh connectivity and boundary vertices remain fixed as the energy is minimized. Also, in contrast to the methods of [2] and [12], the cost function we minimize is explicitly designed to achieve the aim of well-centeredness. This section describes the energy we minimize, which is the main component of our method.

Before describing the energy we note that at times the mesh connectivity or boundary vertices of an initial mesh are defined in such a way that no well-centered mesh exists. For such cases one can apply a preprocessing algorithm to update the mesh connectivity. Section 6 discusses this problem in more detail.

In the proof of Thm. 4.1 we see that in order for a simplex  $\sigma^n$  to be  $n$ -well-centered, the circumcenter  $c(\sigma^n)$  must lie on the same side of facet  $\sigma_i^{n-1}$  as vertex  $v_i$ . To convert this discrete variable into something quantitative we introduce the function  $h(v_i, \sigma^n)$ , the signed distance from  $c(\sigma^n)$  to  $\text{aff}(\sigma_i^{n-1})$  with the convention that  $h(v_i, \sigma^n) > 0$  when  $c(\sigma^n)$  and  $v_i$  are on the same side of  $\text{aff}(\sigma_i^{n-1})$ . The magnitude of  $h(v_i, \sigma^n)$  can be computed as the distance between  $c(\sigma^n)$  and  $c(\sigma_i^{n-1})$ , and its sign can be computed by testing whether  $c(\sigma^n)$  and  $v_i$  have the same orientation with respect to  $\text{aff}(\sigma_i^{n-1})$ . A mesh is  $n$ -well-centered if and only if  $h(v_i, \sigma^n) > 0$  for every vertex  $v_i$  of every  $n$ -simplex  $\sigma^n$  of the mesh.

We divide the quantity  $h(v_i, \sigma^n)$  by the circumradius  $R(\sigma^n)$  to get a quantity that does not depend on the size of the simplex  $\sigma^n$ . We expect a cost function based on  $h(v_i, \sigma^n)/R(\sigma^n)$  to do a better job than the basic  $h(v_i, \sigma^n)$  at preserving properties of the initial mesh. In particular, the grading (relative sizes of the elements) of the initial mesh should be preserved better with  $h/R$  than with  $h$ . Sazonov et al. have also noticed that cost functions based on the quantity  $h/R$  may be helpful in quantifying well-centeredness [32].

Note that  $-1 < h(v_i, \sigma^n)/R(\sigma^n) < 1$  for finite  $\sigma^n$ , because  $R(\sigma^n)^2 = h(v_i, \sigma^n)^2 + R(\sigma_i^{n-1})^2$ . Instead of using the quantity  $h/R$  directly, we consider the function

$$f_n(\sigma^n) = \max_{\text{vertices } v \in \sigma^n} \left| \frac{h(v, \sigma^n)}{R(\sigma^n)} - k_n \right|,$$

where  $0 < k_n \leq 1$  is a constant that may depend on the dimension  $n$  of the simplex. The advantage of minimizing  $f_n$  as opposed to maximizing  $h/R$  is that if  $k_n$  is chosen properly, the measure penalizes simplex vertices where  $h/R$  approaches 1 (e.g., small angles of triangles and sharp points of needle tetrahedra) as well as vertices where  $h/R \leq 0$ .

We want to choose  $k_n$  so that  $f_n(\sigma^n)$  is minimized when  $\sigma^n$  is the regular  $n$ -simplex. Taking  $k_n = 1/n$  may seem like a good choice because it is clear that the regular simplex minimizes  $f_n$ . (When  $k_n = 1/n$ ,  $f_n(\sigma^n) = 0$  for the regular  $n$ -simplex  $\sigma^n$ ). We show in Lemma 5.1, however, that the regular simplex minimizes  $f_n$  for any  $1 \geq k_n \geq 1/n$ .

LEMMA 5.1. *For  $k_n \geq 1/n$ , the measure  $f_n(\sigma^n)$  is minimized when  $\sigma^n$  is a regular simplex.*

*Proof.* Suppose that  $k_n \geq 1/n$ . For the regular simplex, then,  $f_n(\sigma^n) = k_n - 1/n$ . Thus it suffices to show that for any simplex  $\sigma^n$  there exists a vertex  $v$  such that  $h(v, \sigma^n) \leq R(\sigma^n)/n$ ; at such a vertex we have

$$\left| \frac{h(v, \sigma^n)}{R(\sigma^n)} - k_n \right| = k_n - \frac{h(v, \sigma^n)}{R(\sigma^n)} \geq k_n - \frac{1}{n}.$$

We have seen that for a simplex that is not  $n$ -well-centered, there exists a vertex  $v$  with  $h(v, \sigma^n) \leq 0$ , so it remains to prove this for simplices that are  $n$ -well-centered.

Suppose  $\sigma^n$  is  $n$ -well-centered. Let  $h := \min_i h(v_i, \sigma^n)$ . Consider a sphere  $S^{n-1} \subset \text{aff}(\sigma^n)$  with center  $c(\sigma^n)$  and radius  $h$ . We claim that  $\sigma^n$  contains the sphere  $S^{n-1}$ . Indeed, for each facet  $\sigma_i^{n-1}$  of  $\sigma^n$ , since the radius of  $S^{n-1}$  is  $h \leq h(v_i, \sigma^n)$  we have that the sphere  $S^{n-1}$  is contained in the same half space as  $c(\sigma^n)$  and  $v_i$ . Thus the sphere is contained in the intersection of half spaces that defines the simplex, i.e., is contained in the simplex.

It follows, then, that  $h \leq r(\sigma^n)$  where  $r(\sigma^n)$  is the inradius of  $\sigma^n$ . We know that  $h/R \leq r/R \leq 1/n$  and that equality is achieved for only the regular simplex. (The inequality  $r/R \leq 1/n$  is proved in [25], among others.)  $\square$

In light of Lemma 5.1, taking  $k_n = 1/2$ , independent of  $n$ , is a good strategy, because for  $k_n = 1/2$  the cost function  $f_n$  will prefer any  $n$ -well-centered simplex to any simplex that is not  $n$ -well-centered, and among all  $n$ -well-centered simplices,  $f_n$  will prefer the regular simplex over all others. We use  $k_n = 1/2$  for all of the results discussed in Section 7.

For  $k_n > 0$  the objective of  $n$ -well-centeredness is achieved when  $|h/R - k_n| < k_n$  at every vertex of every simplex  $\sigma^n$ . (Note that this is not a necessary condition if  $k_n < 1/2$ .) Our goal, then, is to minimize  $|h/R - k_n|$  over all vertices and all simplices, driving it below  $k_n$  at every vertex of every simplex. It could be effective to work directly with

$$E_\infty(\mathcal{M}) = E_\infty(\mathcal{V}, \mathcal{T}) = \max_{\substack{\text{simplices } \sigma^n \in \mathcal{T} \\ \text{vertices } v_i \in \sigma^n \cap \mathcal{V}}} \left| \frac{h(v_i, \sigma^n)}{R(\sigma^n)} - \frac{1}{2} \right|, \quad (5.1)$$

but we choose instead to minimize an approximation to  $2E_\infty$  given by

$$E_p(\mathcal{M}) = E_p(\mathcal{V}, \mathcal{T}) = \sum_{\substack{\sigma^n \in \mathcal{T} \\ v_i \in \sigma^n \cap \mathcal{V}}} \left| \frac{2h(v_i, \sigma^n)}{R(\sigma^n)} - 1 \right|^p, \quad (5.2)$$

where  $p$  is a parameter.  $\mathcal{M}$  here stands for a mesh consisting of vertices  $\mathcal{V}$  with particular coordinates and a connectivity table  $\mathcal{T}$  that describes which groups of vertices form simplices. Note that  $\lim_{p \rightarrow \infty} (E_p(\mathcal{M}))^{1/p} = 2E_\infty(\mathcal{M})$ , so  $E_p(\mathcal{M})$  is indeed an approximation to  $2E_\infty(\mathcal{M})$ . The factor of 2 is included for numerical robustness. The parameter  $p$  influences the relative importance of the worst vertex-simplex pair compared to the other vertex-simplex pairs in computing the quality of the mesh as a whole. It is convenient to choose  $p$  as a positive even integer, since the absolute value need not be taken explicitly in those cases.

As stated, the measure  $E_p(\mathcal{M})$  leaves some ambiguity in the case of a degenerate simplex, which may occur in a computational setting. For several reasons, including a desire to maintain upper semicontinuity of the cost function, we use the convention

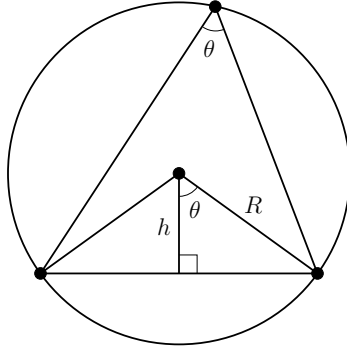


FIG. 5.1. For a triangle,  $h/R = \cos(\theta)$ .

that any degenerate simplex, even one with coincident vertices, has its circumcenter at infinity and  $h/R = -1$ .

Figure 5.1 shows the quantities  $h$  and  $R$  in a sample triangle. We see in the figure that  $\cos(\theta) = h/R$ . Thus (5.2) is a generalization of the energy

$$E_p(\mathcal{M}) = E_p(\mathcal{V}, \mathcal{T}) = \sum_{\theta \in \mathcal{M}} |2 \cos(\theta) - 1|^p, \quad (5.3)$$

which is a constant multiple of the energy the authors proposed earlier for achieving well-centeredness of planar triangle meshes [40]. In three dimensions the quantity  $h/R$  is related to the cosine of the tetrahedron vertex angle, as discussed in [32].

The cost functions  $E_p$  and  $E_\infty$  are not convex. When designing a cost function for mesh optimization, one might hope to develop a function that is convex, or, if not convex, at least one that has a unique minimum. It is, however, not possible to define an energy that accurately reflects the goals of well-centered meshing and also has a unique minimum. Consider the mesh shown on the left in Fig. 5.2. We suppose that the boundary vertices are fixed, but the interior vertex is free to move. We want to decide where to move the interior vertex in order to obtain a well-centered mesh. The right side of Fig. 5.2 shows where the free vertex can be placed to produce a well-centered mesh. The light gray regions are not allowed because placing the free vertex in those regions would make some boundary angle nonacute. (The dotted lines indicate how the four most important boundary angles influence the definition of this region.) The darker gray regions, shown overlaying the light gray region, are not permitted because placing the interior vertex in those regions would make some angle at the interior vertex nonacute.

If the interior vertex is placed in either of the two small white regions that remain, the mesh will be well-centered. We see that the points permitted for well-centeredness form a disconnected set in  $\mathbb{R}^2$ . Moreover, the mesh is radially symmetric, so there is no way to create an energy that prefers one white region over the other unless we violate the desired property that the energy be insensitive to a rotation of the entire mesh. Any symmetric energy that has minima in only the white regions must have at least two distinct global minima.

In most planar triangle meshes there is an interior vertex  $v$  that has exactly six neighbors, all of which are interior vertices. If all interior vertices are free to move, as we assume in the method we propose, then the six neighbors could be moved into the relative positions that the boundary vertices have in the mesh in Fig. 5.2.

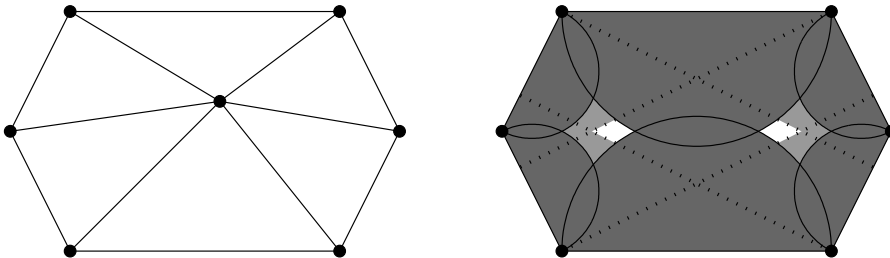


FIG. 5.2. A cost function that accurately reflects the goal of well-centeredness cannot have a unique minimum, because the set of points that make the mesh well-centered may be a symmetric disconnected set.

Moving  $v$  around when its neighbors have such positions should exhibit nonconvexity in whatever cost function we might define.

**6. The Optimal Planar Triangulation.** A variety of our experimental results appears in Section 7 below. The results support the claim that  $E_p$  is an appropriate cost function for quantifying the 2-well-centeredness of a planar mesh. In some cases, though, the mesh connectivity, the fixed boundary vertices, or a combination of the two are specified in such a way that no well-centered mesh exists with the given mesh connectivity and boundary vertices. The simplest example of this is a planar mesh with an interior vertex  $v$  that has fewer than five neighbors. Since the angles around  $v$  sum to  $2\pi$ ,  $v$  has some adjacent angle of at least  $\pi/2$ . The triangle containing that angle is not 2-well-centered. Similarly, a boundary vertex with a boundary angle measuring at least  $\pi/2$  must have enough interior neighbors to divide the boundary angle into pieces strictly smaller than  $\pi/2$ . We will refer to a vertex that does not have enough neighbors as a *lonely* vertex. (In three dimensions, a vertex must have at least 7 incident edges to permit a 3-well-centered mesh, though having 7 neighbors is not sufficient to guarantee that a 3-well-centered neighborhood exists.)

One way to approach problems with mesh connectivity, such as the problem of lonely vertices, is a global mesh connectivity update, i.e., to change the mesh connectivity over the entire mesh. The methods that use Voronoi diagrams [12] and variational triangulations [2] both employ this approach, updating to a Delaunay mesh each time the vertices are relocated. In this section we show that the optimal triangulation of a planar point set with respect to the energy  $E_\infty$  is a minmax triangulation, i.e. a triangulation that minimizes the maximum angle. Note that in general a minmax triangulation is not a Delaunay triangulation. (A Delaunay triangulation is, rather, a maxmin triangulation of a planar point set [37]).

There is an  $O(n^2 \log n)$  time algorithm for computing the minmax angle triangulation of a fixed set of points in the plane [17], so in the plane it might be feasible to recompute the optimal triangulation at every step of our iterative algorithm. It is not clear, however, whether the algorithm of [17] can be generalized into higher dimensions. At the end of this section we discuss some other reasons to avoid recomputing the optimal triangulation after each step of energy minimization.

In the rest of this section we restrict our attention to a given set of vertices  $\mathcal{V}$  in  $\mathbb{R}^2$ , fixed at their initial locations. Given  $\mathcal{V}$  we seek the mesh connectivity  $\mathcal{T}$  that minimizes  $E_\infty(\mathcal{V}, \mathcal{T})$ . Throughout this section, where we refer to mesh connectivity or triangulation it is assumed (often implicitly) that we mean an admissible triangulation, i.e., a triangulation of  $\mathcal{V}$  that covers the convex hull of  $\mathcal{V}$ ,  $\text{conv}(\mathcal{V})$ , and has no

inverted or overlapping triangles. Many of the results would apply when considering a different set of admissible triangulations, but some might need small modifications, depending on the particular set of triangulations admitted.

Since we are working in the plane, the discussion is based on planar angles  $\theta$  and the cost function defined in (5.3) in terms of  $\cos(\theta)$ . In particular we consider the cost functions

$$\begin{aligned} E_{\cos}(\mathcal{V}, \mathcal{T}) &= \max_{\theta \in \mathcal{M}} \{ |2 \cos(\theta) - 1| \} = \lim_{p \rightarrow \infty} \left( \sum_{\theta \in \mathcal{M}} |2 \cos(\theta) - 1|^p \right)^{1/p} \\ E_{\min}(\mathcal{V}, \mathcal{T}) &= \min_{\theta \in \mathcal{M}} \{ \theta \} \\ E_{\max}(\mathcal{V}, \mathcal{T}) &= \max_{\theta \in \mathcal{M}} \{ \theta \}, \end{aligned}$$

where in the latter two cases we require  $\theta \in [0, \pi]$ .

We start by showing that when all triangulations of a planar point set have a maximum angle that is at least  $\pi/2$ , a triangulation minimizing  $E_{\max}$  is also a triangulation that minimizes  $E_{\cos}$ . This claim is readily proved as a corollary of the following proposition.

**PROPOSITION 6.1.** *Let  $f$  be a strictly increasing function of  $\theta$  and  $g$  a nondecreasing function of  $\theta$  for  $\theta \in [0, \pi]$ . If  $E_f(\mathcal{T}) = \max\{f(\theta_i)\}$  and  $E_g(\mathcal{T}) = \max\{g(\theta_i)\}$ , then  $\arg \min E_f \subseteq \arg \min E_g$ .*

*Proof.* For each triangulation  $\mathcal{T}$ , there exists some angle  $\theta_{\mathcal{T}}$  such that  $E_f(\mathcal{T}) = \max\{f(\theta_i)\} = f(\theta_{\mathcal{T}})$ . Thus for all other angles  $\theta$  appearing in triangulation  $\mathcal{T}$ , we have that  $f(\theta_{\mathcal{T}}) \geq f(\theta)$ .

Consider a specific triangulation  $\mathcal{T}_0 \in \arg \min E_f$ . We have  $E_f(\mathcal{T}_0) \leq E_f(\mathcal{T})$  for all triangulations  $\mathcal{T}$ . Thus  $f(\theta_{\mathcal{T}_0}) \leq f(\theta_{\mathcal{T}})$ . Moreover, since  $f$  is a strictly increasing function of  $\theta$ , we can conclude that  $\theta_{\mathcal{T}_0} \leq \theta_{\mathcal{T}}$ . Then since  $g$  is nondecreasing, we have  $g(\theta_{\mathcal{T}_0}) \leq g(\theta_{\mathcal{T}})$  for all triangulations  $\mathcal{T}$ .

Now we claim that for arbitrary triangulation  $\mathcal{T}$  we have  $g(\theta_{\mathcal{T}}) \geq g(\theta)$  for all angles  $\theta$  appearing in triangulation  $\mathcal{T}$ . If this were not the case, then there would exist some angle  $\hat{\theta}$  in  $\mathcal{T}$  with  $g(\hat{\theta}) > g(\theta_{\mathcal{T}})$ . Since  $g$  is nondecreasing, it would follow that  $\hat{\theta} > \theta_{\mathcal{T}}$ , and since  $f$  is strictly increasing, we would have  $f(\hat{\theta}) > f(\theta_{\mathcal{T}})$ . This, however, contradicts our definition of  $\theta_{\mathcal{T}}$ , which states that  $f(\theta_{\mathcal{T}}) = \max\{f(\theta_i)\} \geq f(\hat{\theta})$ . We conclude that the claim is correct.

It follows, then, that  $g(\theta_{\mathcal{T}}) = \max\{g(\theta_i)\} = E_g(\mathcal{T})$  for each triangulation  $\mathcal{T}$ . In particular, the inequality  $g(\theta_{\mathcal{T}_0}) \leq g(\theta_{\mathcal{T}})$  implies that  $E_g(\mathcal{T}_0) \leq E_g(\mathcal{T})$  for all triangulations  $\mathcal{T}$ . By definition,  $\mathcal{T}_0$  is a member of the set  $\arg \min E_g$ .  $\square$

**COROLLARY 6.2.** *If  $f$  is a strictly increasing function of  $\theta$  for  $\theta \in [0, \pi]$ , then  $\arg \min E_f = \arg \min E_{\max}$ .*

*Proof.* The function  $E_{\max}$  is of the form  $E_g$  where  $g$  is the identity function on  $[0, \pi]$ . Since  $g$  is a strictly increasing function, we may apply Proposition 6.1 in both directions to show that  $\arg \min E_f \subseteq \arg \min E_{\max}$  and that  $\arg \min E_{\max} \subseteq \arg \min E_f$ . We conclude that  $\arg \min E_{\max} = \arg \min E_f$ .  $\square$

**COROLLARY 6.3.** *If all triangulations of a set of vertices  $\mathcal{V}$  that cover  $\text{conv}(\mathcal{V})$  have maximum angle at least  $\pi/2$ , then a triangulation minimizing  $E_{\max}$  also minimizes  $E_{\cos}$  and vice versa.*

*Proof.* We can restate the corollary as follows. If  $E_{max} \geq \pi/2$  for all triangulations  $\mathcal{T}$ , then  $\arg \min E_{cos} = \arg \min E_{max}$ . This follows because  $E_{cos}$  is of the form  $E_f$  where  $f = |2 \cos(\theta) - 1|$  is a strictly increasing function on the interval  $[\pi/2, \pi]$ , and  $f(\theta) < f(\pi/2)$  for  $0 < \theta < \pi/2$ . For all practical purposes, we could redefine  $f$  on  $[0, \pi/2)$  to make  $f$  a strictly increasing function on  $[0, \pi]$ . The redefinition would have no effect because for all  $\mathcal{T}$ , the maximal  $f(\theta_i)$  occurs at some  $\theta_i \geq \pi/2$ .

Some care should be taken if we allow meshes that have an angle  $\theta = 0$ , but we know that a triangle with an angle of 0 has some angle measuring at least  $\pi/2$ , even if two of the triangle vertices coincide. Since  $f(\pi/2) = f(0)$ , we may say that on a triangle with angle 0,  $f$  is maximized at the largest angle  $\theta \geq \pi/2$ .  $\square$

It should be clear that the proofs of Prop. 6.1 and Cor. 6.3 do not apply when a triangulation exists with  $E_{max} < \pi/2$ . In that case,  $E_{cos}$  may be maximized at some angle  $\theta \approx 0$  rather than at the largest angle of the mesh. In the next theorem we establish that there is an important relationship between  $\arg \min E_{max}$  and  $\arg \min E_{cos}$  even when a well-centered triangulation exists. (This theorem is the acute angle case of a result from [4], presented here with a different proof.)

**THEOREM 6.4.** *If a 2-well-centered triangulation of a planar point set exists, then that 2-well-centered triangulation is unique and is both the unique Delaunay triangulation of the point set and the unique minmax triangulation of the point set.*

*Proof.* Recall that if the Delaunay complex of a planar point set has a cell that is not triangular, then this cell is a convex polygon with more than three vertices. The vertices of the polygon are all cocircular, and the circumcircle is empty of other points. In this case a (nonunique) Delaunay triangulation may be obtained by triangulating each such polygon arbitrarily. Any such Delaunay triangulation must contain an angle with measure  $\pi/2$  or larger.

This can be argued from considering the possible triangulations of a Delaunay cell that is not triangular. An *ear* of the triangulation of the Delaunay cell is a triangle bounded by one diagonal and two edges of the Delaunay cell. Since the Delaunay cell has four or more vertices, at least two triangles will be ears in any triangulation of the cell. Moreover, we can divide the circumdisk of the Delaunay cell into a pair of closed semidisks in such a way that at least one semidisk completely contains an ear. In an ear contained in a semidisk, the angle along the boundary of the Delaunay cell is at least  $\pi/2$ . We conclude that if the Delaunay complex of a planar point set is not a triangulation, then no completion of the Delaunay complex to a triangulation (i.e., a Delaunay triangulation) yields a 2-well-centered triangulation.

Suppose, then, that a point set permits a 2-well-centered triangulation  $\mathcal{T}_0$ . By Cor. 4.2,  $\mathcal{T}_0$  is a Delaunay triangulation. The Delaunay triangulation is unique in this case (by the argument of the preceding paragraph). Moreover, any other triangulation  $\mathcal{T}$  of the point set has a maximum angle that is at least as large as  $\pi/2$ . (If not,  $\mathcal{T}$  would be 2-well-centered, and, therefore, a Delaunay triangulation, contradicting the uniqueness of the Delaunay triangulation.) We conclude that the minmax triangulation in this case is  $\mathcal{T}_0$  and is unique.  $\square$

Combining Thm. 6.4 with Cor. 6.3 we see that  $\arg \min E_{cos} = \arg \min E_{max}$  in all cases.

Unfortunately, the minmax triangulation and the Delaunay triangulation both have the undesirable property that they may have interior vertices with only four neighbors, i.e., lonely vertices. Figure 6.1 shows a small point set for which the

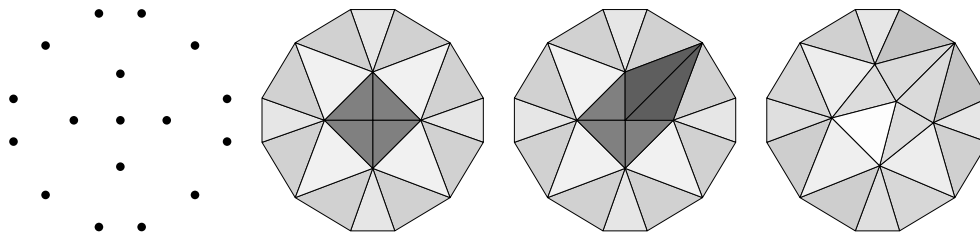


FIG. 6.1. *The minmax triangulation may produce a triangulation in which interior vertices are lonely, even when there are triangulations with no lonely vertices. The sequence of figures shows a point set, the minmax triangulation of the point set, an alternate triangulation of the point set with no lonely vertices, and a 2-well-centered triangulation that is obtained from the alternate triangulation by optimizing  $E_4$ .*

minmax triangulation contains an interior vertex with only four neighbors. In this particular case, the minmax triangulation gives a mesh for which the vertex locations optimize both  $E_\infty$  and  $E_4$ . Thus optimizing  $E_\infty$  or  $E_4$  will not change the mesh, even if we interleave the mesh optimization with recomputing the optimal triangulation.

As long as we maintain the mesh connectivity given by this minmax triangulation, we cannot make the mesh 2-well-centered, regardless of what function we optimize. To address this problem we choose to use an algorithm that preprocesses the mesh, updating the mesh connectivity locally to eliminate lonely vertices. The algorithm we use for the two-dimensional case is outlined in [40]. The preprocessing step applied to the minmax triangulation produces an alternate triangulation of the initial vertex set. (See Fig. 6.1.) For the new triangulation, optimizing  $E_4$  quickly finds a 2-well-centered mesh.

A key reason that we choose to preserve the mesh connectivity throughout the optimization process is that we want to prevent the appearance of lonely vertices during the optimization process. It might be interesting to interleave the energy optimization with a retriangulation step that computed a triangulation that minimizes the maximum angle among all triangulations with no lonely vertices, but we do not know how to compute such a triangulation efficiently. The choice to maintain mesh connectivity during optimization also simplifies the handling of meshes of domains with holes.

**7. Experimental Results.** In this section we give some experimental results of applying our energy minimization to a variety of meshes. All of the initial meshes shown here permit well-centered triangulations, in many cases because the “initial mesh” is the output of some preprocessing algorithm that improves the mesh connectivity, e.g., the preprocessing algorithm described in [40]. The mesh optimization was implemented using the Mesquite library developed at Sandia National Laboratories [8]. We implemented the cost function  $E_p$  by writing a new element-based `QualityMetric` with a constructor accepting the argument  $p$  and summing the energy values on each element with the standard `LPToPTemplate` objective function (with power 1).

We used Mesquite’s implementation of the conjugate gradient method to optimize  $E_p$  on each mesh shown. We did not write code for an analytical gradient, so Mesquite numerically estimated the gradients needed for the conjugate gradient optimization. The optimization was terminated with a `TerminationCriterion` based on the number of iterations, so where the phrase *number of iterations* appears in the experimental

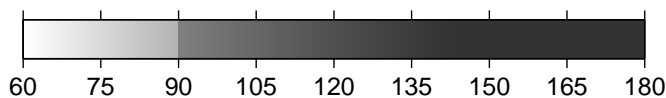


FIG. 7.1. For two-dimensional meshes, the shade of a triangle indicates the measure of its largest angle.

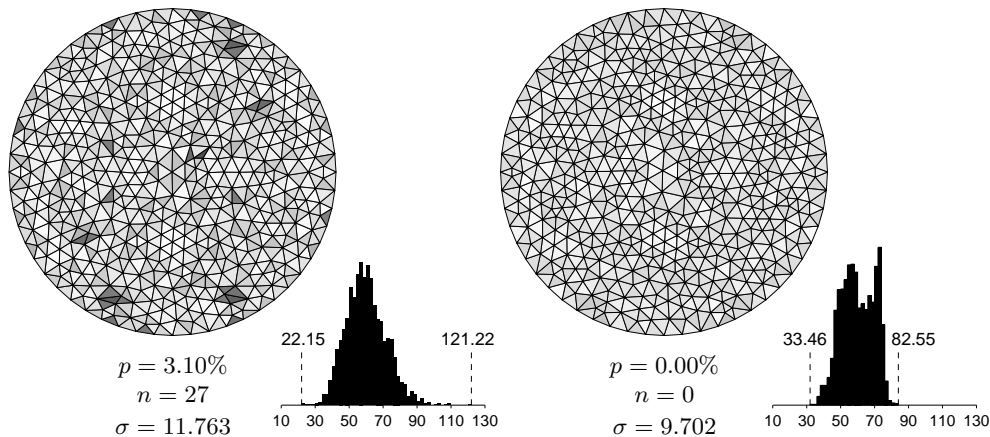


FIG. 7.2. From the initial mesh shown at left, with 3.10% of its triangles nonacute, minimizing  $E_4$  produces the 2-well-centered mesh shown at right in 30 iterations. Histograms of the angles in the mesh are included, with the minimum and maximum angles marked on each histogram. The optimization took 1.61 seconds.

results, it refers to the number of iterations of the conjugate gradient method. For the three-dimensional meshes shown here we used the cost function  $E_p$  for dimension  $n = 3$ , which is designed to find 3-well-centered meshes and is not sensitive to whether the facets of the tetrahedra are acute triangles.

All of the experimental results discussed in this section were run on a desktop machine with a dual 1.42 GHz PowerPC G4 processor and 2 GB of memory. As is often the case with mesh optimization, the algorithm is quite slow. There are certainly opportunities for improving the efficiency of the algorithm as well; the authors suspect that modifying the algorithm to do optimization only in the regions where it is necessary, instead of optimizing over the entire mesh, could improve the efficiency significantly.

*Shading scheme:* For all the two-dimensional meshes shown in this section, we use the scale shown in Fig. 7.1 to determine the shade of each triangle. The shade of a triangle is determined by the measure of the largest angle of the triangle. The shade gets darker as the largest angle increases, with a noticeable jump at  $90^\circ$  so that 2-well-centered triangles can be distinguished from nonacute triangles. For example, the three meshes in Fig. 6.1 use this shading scheme, and it should be easy to identify the triangles that are not 2-well-centered in the first two meshes.

Along with figures of meshes, we include histograms that show the distribution of the angles for two-dimensional meshes. We report near the histogram the percentage  $p$  and the number  $n$  of nonacute triangles in each mesh. The mean of each distribution is  $60^\circ$ , and the standard deviation  $\sigma$  is written near the distribution.

**7.1. Mesh of a Disk.** The mesh of the disk in Fig. 7.2 is small enough that the results of an experiment on the mesh can be visually inspected. Many of the triangles

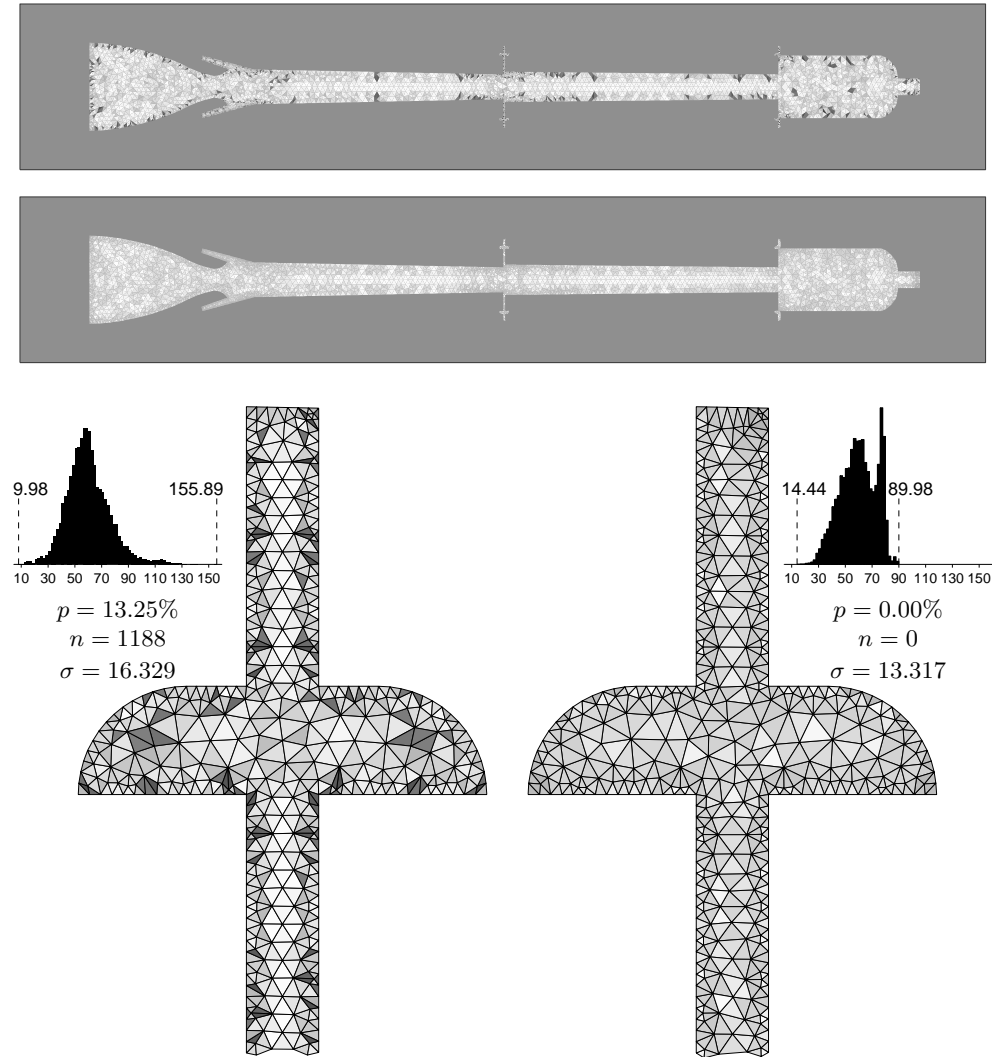


FIG. 7.3. Results of an experiment with a mesh of a 2-dimensional slice of the combustion chamber inside the Titan IV rocket. The initial mesh is displayed at the top. Below it is the result mesh, which was obtained by 1000 iterations minimizing  $E_{10}$  on the mesh. Histograms show the distribution of angles in the initial and final meshes. The zoomed in views of the joint slot (at the top center of the full mesh) show the level of mesh refinement in the regions of higher detail. For the histograms and the zoomed views, the original mesh is on the left, and the result mesh is on the right. The optimization took 805.35 seconds.

are already acute in the initial mesh, but some are not. Based on the shading scheme, we see visually that the result mesh has no nonacute triangles. The histograms of the angles in the mesh confirm this, showing that the maximum angle was reduced from  $121.22^\circ$  to  $82.55^\circ$ , and the minimum angle has increased from  $22.15^\circ$  to  $33.46^\circ$ . The optimization took 1.61 seconds.

**7.2. A Larger Mesh.** In Fig. 7.3 we show results for a larger mesh, a mesh of a two-dimensional slice of the combustion chamber inside the Titan IV rocket. This

mesh, which is based on a mesh that the third author produced from his work for the Center for Simulation of Advanced Rockets, has 8966 triangles. At the top of Fig. 7.3 we show an overview of the entire mesh, with the initial mesh at the very top and the result (after optimizing  $E_{10}$  for 1000 iterations) just below it. These meshes are drawn without showing element edges, because even the thinnest possible edges would entirely obscure some parts of the mesh. The background color helps define the boundary of the mesh by providing contrast with the light gray elements.

Below the mesh overview is a zoomed view of the top center portion of the mesh, which represents a portion of a joint slot of the titan IV rocket. Figure 7.3 also includes histograms of the angle distribution of the full mesh before and after the optimization. The angle histogram and zoomed portion for the initial mesh are shown on the left, and for the optimized mesh are shown on the right.

In the initial mesh there are 1188 nonacute triangles ( $\approx 13.25\%$  of the triangles), with a maximum angle around  $155.89^\circ$ . The result mesh has a maximum angle of  $89.98^\circ$ , and all but 143 triangles ( $\approx 1.59\%$ ) have maximum angle below  $85^\circ$ . Of the 143 triangles that have angles above  $85^\circ$ , 14 have all three vertices on the boundary and are thus completely specified by the boundary. One example of this is in the upper left corner of the zoomed view, where there is a triangle that looks much like an isosceles right triangle. Another 60 triangles are forced to have triangles larger than  $85^\circ$  because they are part of a pair of triangles along a part of the boundary with small but nonzero curvature. There are four such pairs along each curved boundary in the zoomed view in Fig. 7.3. In fact, all but 4 of the 143 “worst” triangles have at least one boundary vertex, and the remaining 4 triangles each have a vertex that is distance one from the boundary.

**7.3. Some More Difficult Tests.** The next mesh is a mesh of a circular domain with two circular holes. The initial mesh is far from being 2-well-centered, with 61.04% of its triangles nonacute, and a standard deviation  $\sigma \approx 31.238$  for the angle distribution. An initial attempt to make the mesh well-centered was unsuccessful, but two slightly different strategies, described later, do produce a well-centered mesh. The initial mesh and its angle histogram are shown in Fig. 7.4 (left) along with the result of minimizing  $E_4$  on the mesh for 500 iterations (right). In this case, the optimization took 88.70 seconds. Comparing the optimized mesh to the initial mesh we see that the quality has improved; the percentage of nonacute triangles is reduced, the standard deviation has improved, and many of the largest angles have been reduced.

Unfortunately, some of the smallest angles of the initial mesh have also gotten smaller in the optimized mesh. In fact, four angles got so small that their triangles became inverted in the optimized mesh. The inverted triangles are too thin to actually see, but there is one pair near the top right of the mesh and one pair near the bottom left. The energy value required to invert a triangle is fairly large, but for large meshes or meshes with a high percentage of bad triangles, improvements at other locations in the mesh may be significant enough to overcome the cost of triangle inversion for a small number of the triangles in the mesh, and using the basic energy  $E_p$  can lead to inverted triangles. Triangle inversion can be prevented by including an inversion barrier in the cost function.

**Energy combined with inversion barrier.** Modifying the energy by introducing a term that has a barrier against inversion, i.e., a term for which the energy value goes to infinity as a triangle moves towards becoming degenerate, is probably the best way to handle the problem of triangles that would become inverted with the basic  $E_p$ . The `IdealWeightInverseMeanRatioQualityMetric` provided by Mesquite is a

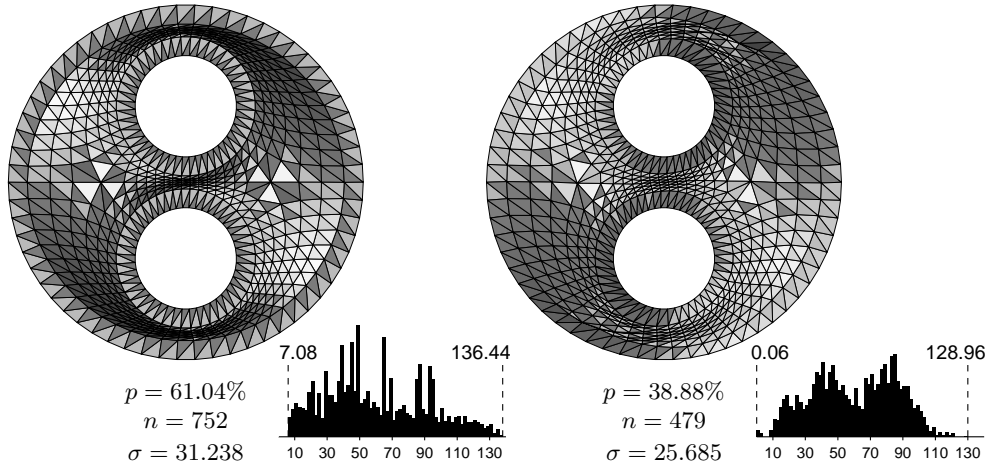


FIG. 7.4. A first attempt at energy minimization applied to the two holes mesh on the left does not yield a well-centered mesh. Result after 500 iterations of  $E_4$  minimization is shown on the right. The optimization took 88.70 seconds. The result mesh has some inverted triangles which are too thin to be seen. In subsequent figures we show several strategies for producing a well-centered configuration.

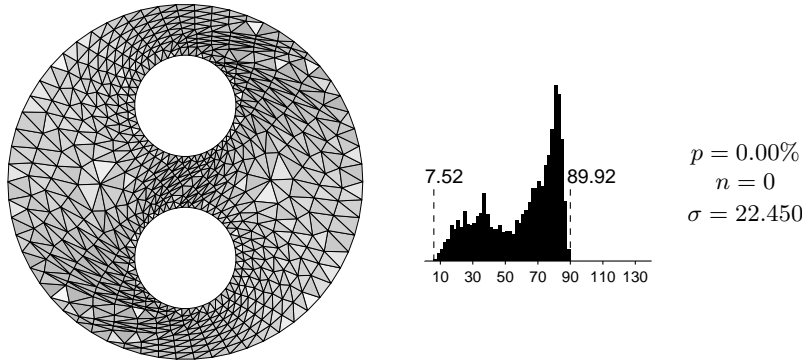


FIG. 7.5. A 2-well-centered mesh of the two holes domain conforming to the mesh connectivity and boundary vertices of the original two holes mesh shown in Fig. 7.4. The mesh was obtained using slightly modified cost functions  $\tilde{E}_p$  that have a barrier against triangle inversion. The optimization procedure was 500 iterations of  $\tilde{E}_4$  followed by 500 iterations of  $\tilde{E}_6$  followed by 500 iterations of  $\tilde{E}_{10}$ . Total optimization time was 115.37 seconds.

cost function that has an implicit barrier against inversion [28]. Let  $E_{\text{imr}}$  represent the cost function associated with the `IdealWeightInverseMeanRatio`. One can take a linear combination of the energy  $E_p$  with  $E_{\text{imr}}$  to create a new energy that has a barrier against inversion and, depending on the coefficients, is still very much like  $E_p$ . We have found that the energy  $\tilde{E}_p := 100E_p + E_{\text{imr}}$  is often effective in cases where the basic  $E_p$  leads to inverted triangles. For this problem, for example, using  $\tilde{E}_p$  gives a well-centered result with no inverted triangles. Starting from the initial mesh and applying 500 iterations of  $\tilde{E}_4$  followed by 500 iterations of  $\tilde{E}_6$  and 500 iterations of  $\tilde{E}_{10}$  produced the 2-well-centered mesh of the original domain displayed in Fig. 7.5. The optimization took  $37.37 + 36.79 + 41.21 = 115.37$  seconds.

**Improved boundary vertex locations.** Another way to get a well-centered

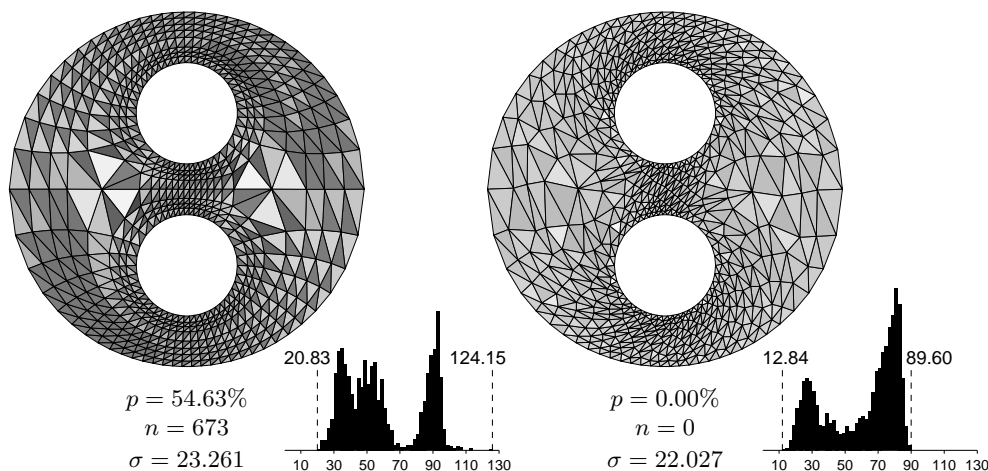


FIG. 7.6. This mesh has the same mesh connectivity as the initial mesh in Fig. 7.4, but the vertices along the boundary (and in the interior) have been moved. The 2-well-centered mesh on the right was obtained in 18.03 seconds with 200 iterations of  $E_6$  minimization.

mesh from this initial mesh is to make the optimization problem easier by changing the location of the boundary vertices. The mesh on the left in Fig. 7.6 has the same mesh connectivity as the initial two holes mesh from Fig. 7.4, but the vertices along the boundary have moved. In the initial mesh the vertices along each boundary were equally spaced, but in this case, the vertices on the outer boundary are more dense at the north and south and less dense at the east and west. The vertices along the inner boundary curves have also moved a bit. For this mesh we use the basic energy  $E_6$ , reaching a well-centered configuration by 200 iterations. The result, obtained in 18.03 seconds, appears on the right in Fig. 7.6.

**Different mesh of the same domain.** The difficulty of finding a 2-well-centered mesh is primarily due to the combined constraints of the mesh connectivity of the initial mesh and the locations of the boundary vertices. The shape of the domain or the fact that the domain is not simply connected are not inherently difficult for the problem of 2-well-centered triangulation. When separated from the mesh connectivity of the initial mesh, the location of the boundary vertices are not a problem either. We demonstrate this by an experiment on the same domain with a completely different mesh that has the same set of boundary vertices and the same boundary vertex locations as the meshes of Figs. 7.4 and 7.5. The experiment, shown in Fig. 7.7, produced a mesh of the domain with maximum angle around  $79.50^\circ$  by optimizing  $E_8$  for 100 iterations. The optimization took 7.44 seconds.

**7.4. A Graded Mesh.** The two holes mesh of Fig. 7.4 and the mesh in Fig. 7.3 related to the titan rocket are both graded meshes. However, the gradation of those meshes was controlled partly by the size of elements on the boundary and by the geometry of the mesh. In Fig. 7.8 we show the results of applying energy minimization to a mesh of the square with an artificially induced gradation. The initial mesh and angle histogram appear at left in Fig. 7.8. The nearly converged result produced by 30 iterations minimizing  $E_4$  is displayed to its right.

The initial size of the triangles of a mesh is not always preserved well when optimizing the energy. We expect, however, that the energy will generally preserve

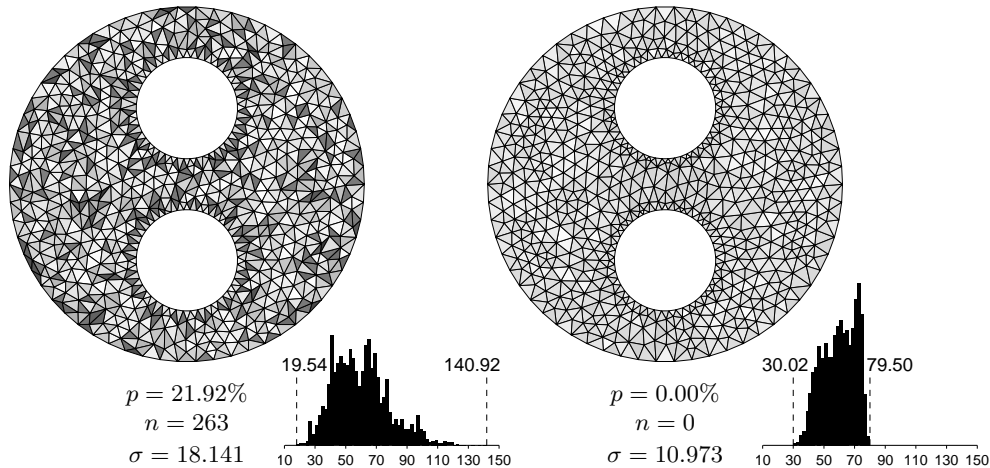


FIG. 7.7. This is a mesh with the same domain and same boundary vertices as the mesh in Fig. 7.4. The 2-well-centered mesh on the right was obtained from the mesh on the left in 7.44 seconds by minimizing  $E_8$  for 100 iterations. The high-quality result shows that the difficulty of getting a 2-well-centered mesh in Fig. 7.4 is not due solely to the domain or the boundary vertices. The initial mesh for this experiment was generated using the freely available software Triangle [36] and heuristics for improving the mesh connectivity.

the grading of an input mesh if the initial mesh is relatively high quality. This hypothesis stems from the observation that the energy is independent of triangle size, the idea that the mesh connectivity combined with the property of 2-well-centeredness somehow controls the triangle size, and the supporting evidence of this particular experiment.

Thus optimizing graded meshes is a useful application of our algorithm; there are no known provably correct algorithms for creation of graded acute-angled triangulations of planar domains. The recent algorithm of [21] has produced graded acute triangulations in a variety of experiments, but in all cases we have tried, we have been able to improve the quality of their triangulations (Section 7.5). Moreover, their algorithm is not known to generalize to higher dimensions.

**7.5. Mesh of Lake Superior.** The Lake Superior domain, with its complicated shape, has appeared in many papers about quality meshing. We include an example optimizing a mesh of this well-known domain. The initial mesh is already 2-well-centered in this experiment, but we show that we can improve its quality with our optimization algorithm. The results are represented graphically in Fig. 7.9.

The initial acute-angled mesh is from the work of Erten and Üngör [21] on generating acute 2-D triangulations with a variant of Delaunay refinement. The initial mesh has a maximum angle of  $89.00^\circ$  with 174 triangles having angles larger than  $88.00^\circ$ . Directly optimizing  $E_{10}$  on the initial mesh, Mesquite finds a local minimum of  $E_{10}$  after 6.63 seconds (21 iterations). The local minimum has exactly one non-acute triangle (maximum angle  $91.03^\circ$ ) and only 40 triangles having angles larger than  $88.00^\circ$ . The angle histogram for this result is included in Fig. 7.9 at top center. The mesh is visually very similar to the initial mesh and does not appear in this paper.

If we start by optimizing  $E_4$  and follow that by optimizing  $E_{10}$  we obtain a local (perhaps also global) minimum of  $E_{10}$  with with much lower energy than the result obtained by directly optimizing  $E_{10}$ . The result of this optimization process is shown

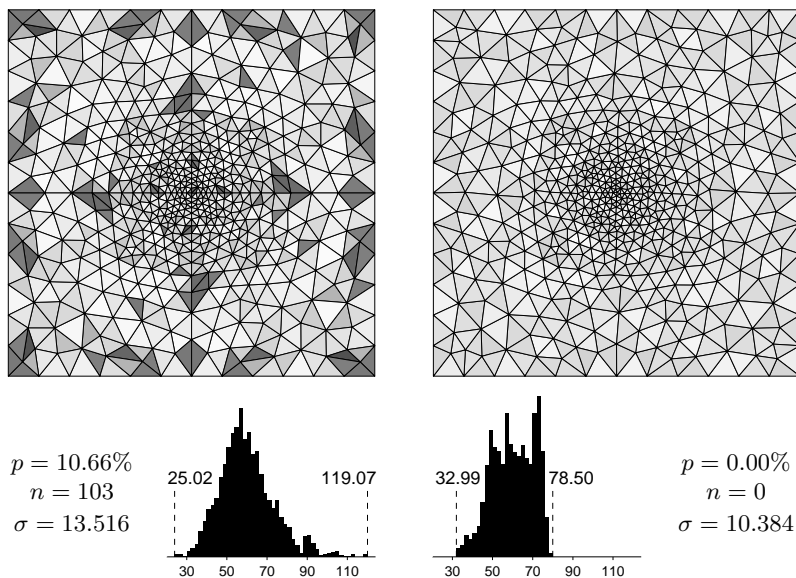


FIG. 7.8. For this graded mesh of the square, minimizing  $E_4$  on the initial mesh (left) produces a 2-well-centered mesh (right) that has grading similar to the initial mesh. The optimization ran for 30 iterations, completing in 2.16 seconds.

on the right in Fig. 7.9. The optimization took 131.48 seconds total; Mesquite spent 102.81 seconds (453 iterations) finding a minimum of  $E_4$  and 28.67 seconds (125 iterations) finding a minimum of  $E_{10}$ .

Laplacian smoothing is a popular mesh optimization technique that was first used for structured meshes with quadrilateral elements and later generalized to triangle meshes [43]. A brief description of Laplacian smoothing is given in [22]. We compare our mesh optimization technique with Laplacian smoothing, using the implementation of Laplacian smoothing provided by the Mesquite library. The result of Laplacian smoothing on the Lake Superior mesh is shown in Fig. 7.10. The optimization was terminated after 100 iterations, which is near convergence. The run time was 1.31 seconds. The maximum angle in the result is  $109.27^\circ$  and more than 4% of the triangles are nonacute.

The result of optimizing the Lake Superior mesh with Laplacian smoothing is typical of the results obtained with Laplacian smoothing. We performed experiments with Laplacian smoothing on all of the 2-D meshes presented in this paper, and no mesh became well-centered except for the mesh of the square in Fig. 7.8, where Laplacian smoothing produced a mesh with maximum angle  $87.54^\circ$  compared to the maximum angle of  $78.50^\circ$  obtained by our method. In most cases the percentage of nonacute triangles after Laplacian smoothing was between 1% and 5%, but for the meshes in Figs. 7.4, 7.5, and 7.6, the percentage of nonacute triangles was much higher, getting as high as 48.70% for the mesh in Fig. 7.6. Clearly the traditional Laplacian smoothing is not an appropriate tool for finding acute triangulations.

**7.6. Colombia, India, and Thailand.** We end our 2-D experimental results with a collection of three large meshes of complicated geographical domains. The experiments are summarized in 7.11. For each of these meshes the optimization started by minimizing  $\tilde{E}_8$  for 500 iterations and then proceeded by minimizing  $E_8$ , running

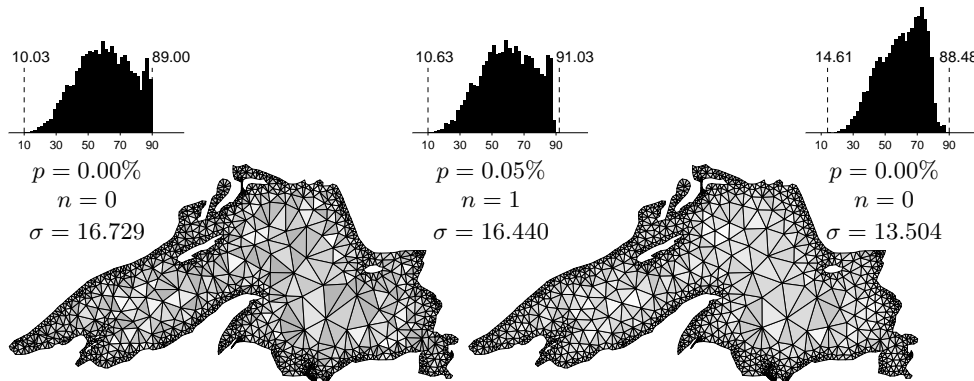


FIG. 7.9. Result for a mesh of Lake Superior. The initial mesh shown on the left is a 2-well-centered mesh from [21]. The improved mesh shown on the right was obtained by first optimizing  $E_4$  and then optimizing  $E_{10}$ . The angle histogram at top center shows the result of optimizing  $E_{10}$  directly on the initial mesh. Many of the angles that were near  $90^\circ$  have dropped to below  $80^\circ$ .

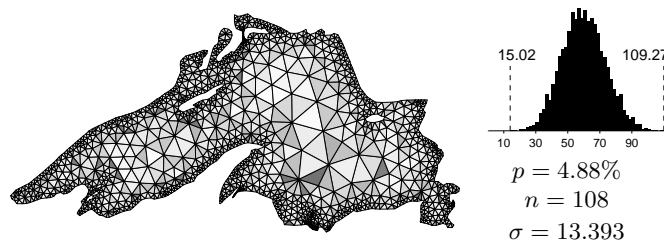


FIG. 7.10. Result of applying Laplacian smoothing to the initial acute mesh of Lake Superior (left side of Fig. 7.9). More than 4% of the triangles become nonacute, and the maximum angle increases to  $109.27^\circ$ .

500 iterations at a time until the mesh became well-centered. After the mesh became well-centered, we used one more round of 500 iterations minimizing  $E_8$  to get some additional improvement in the angle distribution.

The total number of iterations for the meshes was 2000 iterations for Colombia, 3500 iterations for India, and 3000 iterations for Thailand, with total optimization times of 5284.01 seconds, 16162.20 seconds, and 8263.82 seconds. The meshes are quite large, with 38233 triangles, 62370 triangles, and 34562 triangles respectively. In each case, more than 19% of the triangles are nonacute in the initial mesh, and the maximum angle is larger than  $160^\circ$ , yet the optimization finds a well-centered result. It is also clear that the optimization preserves the gradual change in element size from the tiny triangles needed to resolve the boundaries to the much larger triangles in the interiors of the meshes.

**7.7. 3D Meshes.** For tetrahedral meshes, the question of whether the mesh connectivity permits a well-centered mesh is more difficult than its two-dimensional analogue [41]. In part because we do not yet have an effective preprocessing algorithm for tetrahedral meshes, many of our optimization experiments in three dimensions have been limited to meshes with carefully designed mesh connectivity. The mesh shown in Fig. 7.12 is one of these meshes. The shading of the tetrahedral elements in Fig. 7.12 represents the shadows that would result from viewing the faceted object

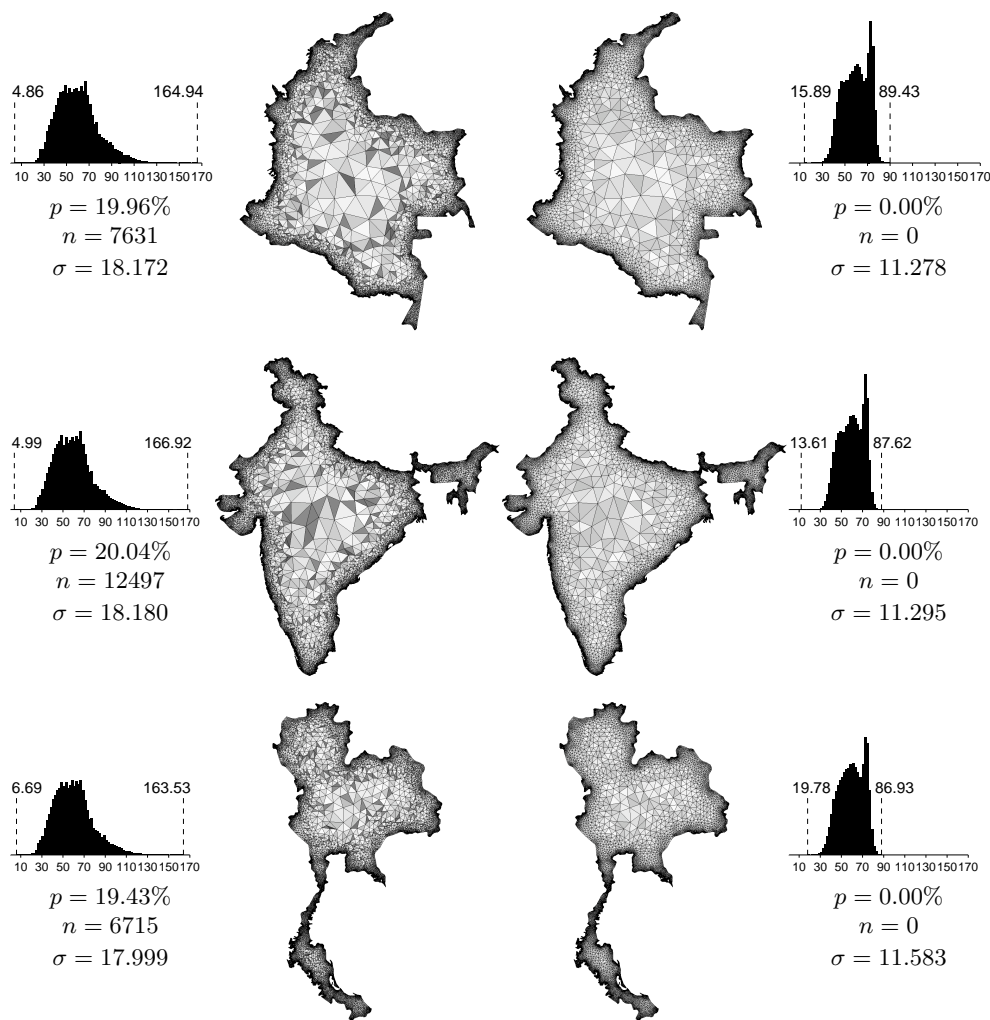


FIG. 7.11. These meshes of complicated geographical boundaries were optimized with an initial 500 iterations of  $E_8$ , followed by successive rounds of 500 iterations minimizing the basic  $E_8$ . The optimization produces well-centered meshes that preserve the grading of the input meshes. (The dark regions near the boundaries of the meshes come from the agglomeration of the edges of triangles that are too small to be seen.) The data for the geographical boundaries was produced using the `CountryData[]` command of Mathematica. Initial meshes were constructed from the input polygons using `Triangle` [36] and heuristics for improving the mesh connectivity.

under a light source; it has nothing to do with the quality of the elements of the mesh. The full mesh is a mesh of the three-dimensional cube with 430 tetrahedra. Figure 7.12 uses a cutaway view to display some of the elements in the interior of the mesh.

Although the initial mesh was carefully designed to have good mesh connectivity (e.g., each vertex has at least 10 incident edges) and a high-quality surface mesh, it was not 3-well-centered. In fact, 22.33% of the tetrahedra are not 3-well-centered. Optimizing  $E_{16}$  for 3.92 seconds (20 iterations) produced a 3-well-centered mesh. Even though the initial mesh was carefully designed, the optimization result is nontriv-

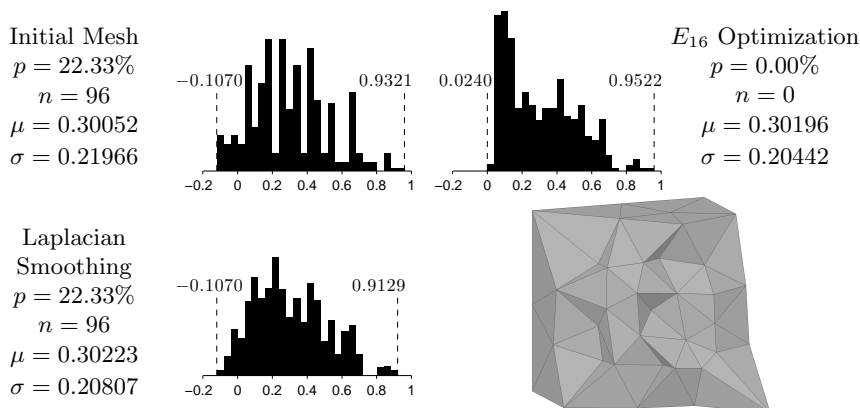


FIG. 7.12. A cutout view showing the interior of a 3-well-centered mesh of the cube. The mesh is the result of 3.92 seconds (20 iterations) of optimizing  $E_{16}$  on an initial mesh for 22.33% of the tetrahedra were not 3-well-centered. Recall that a tetrahedron  $\sigma^3$  is 3-well-centered if and only if  $h(v, \sigma^3)/R(\sigma^3) > 0$  for each vertex  $v$  of  $\sigma^3$ . For a regular tetrahedron,  $h/R = 1/3$ . The  $h/R$  distributions for the initial mesh, the result of optimizing  $E_{16}$ , and the result of Laplacian smoothing show the superiority of our method for finding 3-well-centered meshes.

ial. We compared optimization of  $E_{16}$  to the Mesquite implementation of Laplacian smoothing, applying Laplacian smoothing to the initial mesh and running it until it converged after 60 iterations (0.14 seconds). The result of Laplacian smoothing is a mesh in which 22.33% of the tetrahedra are not 3-well-centered. Figure 7.12 includes the  $h(v, \sigma)/R(\sigma)$  distributions for the initial mesh, the mesh after optimizing  $E_{16}$ , and the mesh resulting from Laplacian smoothing. Near each histogram we show the percentage  $p$  and number  $n$  of tetrahedra (not  $h/R$  values) that are not 3-well-centered, and we report the mean  $\mu$  and standard deviation  $\sigma$  of the distribution of  $h/R$  values.

It is worth noting that, because of its difficulty, obtaining well-centered triangulations and/or acute triangulations of 3-dimensional objects is significant no matter how they are obtained. In our other work we have made use of the optimization techniques developed in this paper to construct well-centered triangulations of several simple three-dimensional shapes [39] and to constructively prove the existence of an acute triangulation of the 3-dimensional cube [42], solving an open problem mentioned in [19] and [7].

**8. Conclusions and Research Questions.** This paper shows that an  $n$ -well-centered simplex can be characterized in terms of the equatorial balls of its facets and uses this alternate characterization to prove that an  $n$ -well-centered mesh in  $\mathbb{R}^n$  is a Delaunay mesh. The paper introduces the related cost functions  $E_\infty$  and  $E_p$  that quantify the well-centeredness of triangulations in any dimension, extending the function introduced in [40]. Some properties of the cost function are discussed, and it is shown that a cost function quantifying well-centeredness must be nonconvex.

After introducing the cost function, the paper shows that the minmax angle triangulation is the optimal triangulation with respect to the  $E_\infty$  energy and discusses why our algorithm uses the local preprocessing algorithm of [40] instead of computing the maxmin triangulation after each step of optimization. The discussion raises the interesting research question of how to efficiently compute (and recompute) a triangulation that minimizes the maximum angle among triangulations with no lonely vertices.

The task of developing a local preprocessing algorithm that works in dimensions higher than 2 is another important research objective. A simple and complete characterization of the mesh connectivity requirements for a vertex and its one-ring in a tetrahedral mesh in  $\mathbb{R}^3$  to be 3-well-centered would be helpful. We have made a start for such a characterization in [41], where we have discovered some beautiful connections to the triangulation of the spherical link of the one ring.

The experiments of Section 7 show that the proposed cost function can be effective in finding a well-centered triangulation for meshes that permit such triangulations. The optimization problem in the context of our nonconvex cost functions  $E_p$  is a difficult problem, though, and Mesquite does not always find a global minimum of the energy. While it is easy to show that our gradient descent type algorithm converges to a local stationary point, it would be nice to have an optimization method guaranteed to find a global minimum of the energy. This however is a very hard problem and typical of the difficulties faced by other iterative algorithms for mesh optimization. For example, for the vastly popular iterative algorithms for centroidal Voronoi tessellations [12] and their variations [13, 14], restricted convergence results have only recently started appearing [11, 18]. Similarly, a convergence proof for variational tetrahedral meshing [2] is known for only one rings, although the algorithm is very useful in practice.

It would also be worthwhile to improve the efficiency of our optimization. In particular, it would be interesting to study methods for localizing the energy and applying optimization in only those specific areas where it is needed. Besides possibly making the optimization more efficient, localizing the energy would make it easier to parallelize the algorithm. The experiment in Section 7.3 that made the optimization easier by repositioning the boundary vertices suggests that using a constrained optimization with boundary vertices free to move along the boundary could make the optimization more effective.

It is also possible that the cost function could be improved. Using a linear combination of  $E_{\text{imr}}$  with  $E_p$  was effective for the two holes mesh of Section 7.3 and the geographical meshes in Section 7.6, but the coefficients of the linear combination were chosen quite arbitrarily, and there may be other, better ways to prevent element inversion. There were also some experiments which needed to use  $E_p$  with more than one parameter  $p$  in order to find a nice result. Taking a linear combination of  $E_p$  for different powers of  $p$  might be effective for those situations and perhaps more generally.

Since the original submission of this manuscript, the authors have become aware that Sazanov et al. generated a 3-well-centered mesh of a spherical layer by repeating the near-boundary triangulation of their mesh stitching approach without stitching to an ideal mesh [34]. Generalizing their construction to more complicated 3-D domains is another interesting direction for research.

To summarize the paper briefly, our generalized characterization of well-centeredness offers, for the first time, a direction in which planar acute triangulations may be generalized. More complex three dimensional experiments will have to await a better preprocessing and better mathematical understanding of the topological obstructions to well-centeredness.

We believe we have shown enough evidence in this and related publications that one can produce simple three dimensional well-centered tetrahedral meshes. In planar domains, it is already possible to produce well-centered triangulations with or without holes and gradations, for complex domains. It is also possible to improve

triangulations that are already acute. Like many other successful mesh optimization algorithms, a convergence theory for well-centered meshing will be discovered eventually, we hope, either by us or by other researchers. For further developments, we felt the need to make available the evidence that well-centered meshes are now possible for experiments, and that there is a useful characterization theory for such meshes.

**Acknowledgment.** We would like to thank Vadim Zharnitsky for useful discussions. We also thank Hale Erten and Alper Üngör for providing us with the Lake Superior mesh. Lastly, we thank the reviewers; their comments led to improvement of the paper.

### References.

- [1] ABRAHAM, R., MARSDEN, J. E., AND RATIU, T. *Manifolds, Tensor Analysis, and Applications*, second ed. Springer–Verlag, New York, 1988.
- [2] ALLIEZ, P., COHEN-STEINER, D., YVINEC, M., AND DESBRUN, M. Variational tetrahedral meshing. *ACM Transactions on Graphics* 24, 3 (2005), 617–625.
- [3] BERN, M., MITCHELL, S., AND RUPPERT, J. Linear-size nonobtuse triangulation of polygons. In *Proceedings of the tenth annual ACM Symposium on Computational Geometry* (New York, 1994), ACM Press, pp. 221–230.
- [4] BERN, M. W., AND EPPSTEIN, D. Mesh generation and optimal triangulation. In *Computing in Euclidean Geometry*, D.-Z. Du and F. K.-M. Hwang, Eds., second ed., no. 4 in Lecture Notes Series on Computing. World Scientific, 1995, pp. 47–123.
- [5] BERN, M. W., EPPSTEIN, D., AND GILBERT, J. Provably good mesh generation. *J. Computer and Systems Sciences* 48, 3 (June 1994), 384–409. Special issue for 31st FOCS.
- [6] BOBENKO, A. I., AND SPRINGBORN, B. A. Variational principles for circle patterns and Koebe’s theorem. *Trans. Amer. Math. Soc.* 356 (2004), 659–689.
- [7] BRANDTS, J., KOROTOV, S., KRÍZEK, M., AND ŠOLC, J. On nonobtuse simplicial partitions. *SIAM Review* 51, 2 (2009), 317–335.
- [8] BREWER, M., DIACHIN, L., KNUPP, P., LEURENT, T., AND MELANDER, D. The mesquite mesh quality improvement toolkit. In *Proceedings of the 12th International Meshing Roundtable* (2003), pp. 239–250.
- [9] COLLINS, C. R., AND STEPHENSON, K. A circle packing algorithm. *Computational Geometry: Theory and Applications* 25, 3 (2003), 233–256.
- [10] DESBRUN, M., HIRANI, A. N., LEOK, M., AND MARSDEN, J. E. Discrete exterior calculus. *arXiv:math.DG/0508341* (August 2005).
- [11] DU, Q., EMELIANENKO, M., AND JU, L. Convergence of the Lloyd algorithm for computing centroidal Voronoi tessellations. *SIAM Journal on Numerical Analysis* 44, 1 (2006), 102–119.
- [12] DU, Q., FABER, V., AND GUNZBURGER, M. Centroidal Voronoi tessellations: applications and algorithms. *SIAM Review* 41, 4 (1999), 637–676.
- [13] DU, Q., GUNZBURGER, M. D., AND JU, L. Constrained centroidal Voronoi tessellations for surfaces. *SIAM Journal on Scientific Computing* 24, 5 (2003), 1488–1506.
- [14] DU, Q., AND WANG, D. Anisotropic centroidal Voronoi tessellations and their applications. *SIAM Journal on Scientific Computing* 26, 3 (2005), 737–761.
- [15] EDELSBRUNNER, H. *Geometry and Topology for Mesh Generation*. Cambridge University Press, 2001.
- [16] EDELSBRUNNER, H., AND SHAH, N. R. Incremental topological flipping works for regular triangulations. *Algorithmica* 15, 3 (March 1996), 223–241.

- [17] EDELSBRUNNER, H., TAN, T., AND WAUPOTITSCH, R. An  $O(n^2 \log n)$  time algorithm for the minmax angle triangulation. *SIAM Journal on Scientific and Statistical Computing* 13, 4 (July 1992), 994–1008.
- [18] EMELIANENKO, M., JU, L., AND RAND, A. Nondegeneracy and weak global convergence of the Lloyd algorithm in  $\mathbb{R}^d$ . *SIAM Journal on Numerical Analysis* 46, 3 (2008), 1423–1441.
- [19] EPPSTEIN, D., SULLIVAN, J. M., AND ÜNGÖR, A. Tiling space and slabs with acute tetrahedra. *Computational Geometry: Theory and Applications* 27, 3 (2004), 237–255.
- [20] ERICKSON, J., GUOY, D., SULLIVAN, J., AND ÜNGÖR, A. Building spacetime meshes over arbitrary spatial domains. In *Proceedings of the 11th International Meshing Roundtable* (2002), Sandia National Laboratories, pp. 391–402.
- [21] ERTEN, H., AND ÜNGÖR, A. Computing acute and non-obtuse triangulations. In *Proceedings of the 19th Canadian Conference on Computational Geometry (CCCG2007)* (August 20–22 2007).
- [22] FIELD, D. A. Laplacian smoothing and Delaunay triangulations. *Communications in Applied Numerical Methods* 4, 6 (1988), 709–712.
- [23] HIRANI, A. N. *Discrete Exterior Calculus*. PhD thesis, California Institute of Technology, May 2003.
- [24] HIRANI, A. N., NAKSHATRALA, K. B., AND CHAUDHRY, J. H. Numerical method for Darcy flow derived using Discrete Exterior Calculus. Tech. Rep. UIUCDCS-R-2008-2937, Department of Computer Science, University of Illinois at Urbana-Champaign, February (Revised October) 2008. Also available as preprint arXiv:0810.3434v1 [math.NA] on arxiv.org.
- [25] KLAMKIN, M. S., AND TSINTSIFAS, G. A. The circumradius-inradius inequality for a simplex. *Mathematics Magazine* 52, 1 (January 1979), 20–22.
- [26] MAEHARA, H. Acute triangulations of polygons. *European Journal of Combinatorics* 23, 1 (2002), 45–55.
- [27] MELISSARATOS, E. A., AND SOUVAINE, D. L. Coping with inconsistencies: A new approach to produce quality triangulations of polygonal domains with holes. In *SCG '92: Proceedings of the Eighth Annual Symposium on Computational Geometry* (New York, NY, USA, 1992), ACM Press, pp. 202–211.
- [28] MUNSON, T. Mesh shape-quality optimization using the inverse mean-ratio metric. *Math. Program.* 110, 3 (2007), 561–590.
- [29] NICOLAIDES, R. A. Direct discretization of planar div-curl problems. *SIAM Journal on Numerical Analysis* 29, 1 (1992), 32–56.
- [30] RAJAN, V. Optimality of the Delaunay triangulation in  $\mathbb{R}^d$ . *Discrete and Computational Geometry* 12, 1 (December 1994), 189–202.
- [31] RUPPERT, J. A Delaunay refinement algorithm for quality 2-dimensional mesh generation. *J. Algorithms* 18, 3 (1995), 548–585.
- [32] SAZONOV, I., HASSAN, O., MORGAN, K., AND WEATHERILL, N. P. Smooth Delaunay–Voronoi dual meshes for co-volume integration schemes. In *Proceedings of the 15th International Meshing Roundtable* (Birmingham, Alabama, September 17–20 2006), Sandia National Laboratories.
- [33] SAZONOV, I., HASSAN, O., MORGAN, K., AND WEATHERILL, N. P. Yee’s scheme for the integration of Maxwell’s equation on unstructured meshes. In *Proceedings of the European Conference on Computational Fluid Dynamics (EC-COMAS CFD 2006)* (2006), P. Wesseling, E. O. nate, and J. Périaux, Eds.
- [34] SAZONOV, I., HASSAN, O., MORGAN, K., AND WEATHERILL, N. P. Generat-

- ing the Voronoi-Delaunay dual diagram for co-volume integration schemes. In *Proceedings of the 4th International Symposium on Voronoi Diagrams in Science and Engineering (ISVD 2007)* (2007).
- [35] SAZONOV, I., WANG, D., HASSAN, O., MORGAN, K., AND WEATHERILL, N. P. A stitching method for the generation of unstructured meshes for use with co-volume solution techniques. *Computer Methods in Applied Mechanics and Engineering* 195, 13-16 (February 2006), 1826–1845.
- [36] SHEWCHUK, J. R. Triangle: Engineering a 2D quality mesh generator and Delaunay triangulator. In *Applied Computational Geometry: Towards Geometric Engineering*, M. C. Lin and D. Manocha, Eds., vol. 1148 of *Lecture Notes in Computer Science*. Springer-Verlag, May 1996, pp. 203–222. From the First ACM Workshop on Applied Computational Geometry.
- [37] SIBSON, R. Locally equiangular triangulations. *The Computer Journal* 21, 3 (March 1978), 243–245.
- [38] ÜNGÖR, A., AND SHEFFER, A. Pitching tents in space-time: Mesh generation for discontinuous Galerkin method. *International Journal of Foundations of Computer Science* 13, 2 (2002), 201–221.
- [39] VANDERZEE, E., HIRANI, A. N., AND GUOY, D. Triangulation of simple 3D shapes with well-centered tetrahedra. In *Proceedings of the 17th International Meshing Roundtable*, R. V. Garimella, Ed. Springer Berlin Heidelberg, Pittsburgh, Pennsylvania, October 12–15 2008, pp. 19–35. Also available as a preprint arXiv:0806.2332v2 [cs.CG] on arxiv.org.
- [40] VANDERZEE, E., HIRANI, A. N., GUOY, D., AND RAMOS, E. Well-centered planar triangulation – an iterative approach. In *Proceedings of the 16th International Meshing Roundtable* (Seattle, Washington, October 14–17 2007), M. L. Brewer and D. Marcum, Eds., Springer, pp. 121–138.
- [41] VANDERZEE, E., HIRANI, A. N., GUOY, D., RAMOS, E., AND ZHARNITSKY, V. Conditions for well-centeredness. Tech. Rep. UIUCDCS-R-2008-2971, Department of Computer Science, University of Illinois at Urbana-Champaign, 2008.
- [42] VANDERZEE, E., HIRANI, A. N., ZHARNITSKY, V., AND GUOY, D. A dihedral acute triangulation of the cube. *Computational Geometry: Theory and Applications Accepted* (2009). Also available as preprint arXiv:0905.3715v3 [cs.CG] on arxiv.org.
- [43] WINSLOW, A. M. An irregular triangle mesh generator. Tech. Rep. UCRL-7880, National Technical Information Service, Springfield, VA, 1964.
- [44] YUAN, L. Acute triangulations of polygons. *Discrete and Computational Geometry* 34, 4 (2005), 697–706.